ELSEVIER

Comput. Methods Appl. Mech. Engrg. 191 (2002) 5287–5314

Computer methods in applied mechanics and engineering

www.elsevier.com/locate/cma

# Bifurcation of elastoplastic solids to shear band mode at finite strain

Ronaldo I. Borja *

*Department of Civil and Environmental Engineering, Stanford University, Stanford, CA 94305-4020, USA*

Received 19 January 2001; received in revised form 22 July 2002

**Abstract**

This paper formulates and implements a finite deformation theory of bifurcation of elastoplastic solids to planar bands within the framework of multiplicative plasticity. Conditions for the onset of strain localization are based on the requirement of continuity of the nominal traction vector, and are described both in the reference and deformed configurations by the vanishing of the determinant of either the Lagrangian or Eulerian acoustic tensor. The relevant acoustic tensors are derived in closed form to examine the localization properties of a class of elastoplastic constitutive models with smooth yield surfaces appropriate for pressure-sensitive dilatant/frictional materials. A link between the development of regularized strong discontinuity and its unregularized counterpart at the onset of localization is also discussed. The model is implemented numerically to study shear band mode bifurcation of dilatant frictional materials in plane strain compression. Results of the analysis show that finite deformation effects do enhance strain localization, and that with geometric nonlinearities bifurcation to shear band mode is possible even in the hardening regime of an associative elastoplastic constitutive model.


*Keywords:* Bifurcation; Elastoplastic solids; Shear bond mode; Finite strain

## 1. Introduction

Strain localization has attracted much research attention lately and is presently in the center of current research interests in many areas of engineering due to its significant influence on the behavior of a vast number of engineering materials. Specific examples demonstrating strain localization phenomena include Lüders bands and necking in metals, shear bands in paraffin, rock faults in marble and sandstone, shear bands in soils, micro-cracking in concrete, and necking in polymers [1–8]. Generally considered a result of material instability [9], strain localization plays a critical role in describing the failure and near-failure responses of many engineering structures.

* Fax: + 1-650-723-7514.
*E-mail address:* borja@stanford.edu (R.I. Borja).

0045-7825/02/$ - see front matter 
PII: S0045-7825(02)00459-0

Instabilities are influenced by existing defects or imperfections in a material that may be viewed otherwise as homogeneous on a larger scale. However, accurate representation of these imperfections are difficult if not impossible. In this paper, we view material instability as resulting from possible bifurcation of the macroscopic, inelastic constitutive behavior. Here, the material in question permits the governing field equations to be satisfied for an alternate field. Significant contributions toward the development of the localization theory have been made by Hadamard [10], Hill [11], Thomas [12], and Mandel [13] within the context of acceleration waves in elastoplastic solids.

A specific instability problem we seek to address concerns the bifurcation of a nonlinear continuum into a planar band where either the velocity gradient field or the velocity field is discontinuous. Current work on this topic has progressed at a very rapid pace, and now has addressed not only the case of elastoplastic responses [14–16] but also the case of hypoplastic responses [17–20]. A complicating factor concerns the incremental nonlinearity of the constitutive response which makes the bifurcation analysis less straightforward. Incremental nonlinearity could arise from the specific type of a constitutive response in which the tangent operator may depend on the velocity gradient, and hence, on the direction of the imposed incremental deformation. In elastoplasticity, incremental nonlinearity could arise at the inception of localization from possible combination of plastic loading and elastic unloading on either side of the band.

A majority of research effort in bifurcation analysis has focused primarily on the geometrically linear case where the deformation is infinitesimal. In general, any result derived from such analysis must be taken with caution since geometric nonlinearities play a very crucial role in the theory of bifurcation [21]. It suffices to recall the Euler buckling of columns to underscore this last statement [22]. In general, geometric effects have a profound impact when the stresses are in the same order of magnitude as the tangential moduli since they tend to destroy the symmetry of the tangent operator, and so are expected to enhance strain localization.

Efforts to generalize the theory of shear band bifurcation to include geometric nonlinearities have been hampered by the lack of well-structured finite deformation theory and algorithm that can be used for general multipurpose numerical codes. The widely used finite deformation theory based on hypoelastic formulation has been the subject of some controversy only settled in recent years [23], both on the theoretical formulation side as well as on the numerical implementation aspects. In localization analysis, where the tangent operator is used directly to detect bifurcation, the lack of a unique objective stress rate to use in the expression for the acoustic tensor renders the resulting bifurcation analysis questionable. Efforts also have been made to cast the infinitesimal plasticity theory to the finite deformation regime via the use of the generalized Lagrangian stresses and strains [24–26]. However, the formulation has not found much success in computer codes, and to date no well-developed algorithm based on this approach is available [22].

Research on finite deformation elastoplasticity based on a multiplicative decomposition of the deformation gradient has received much attention in the computational mechanics community in recent years [23,27–30]. This formulation has a hyperelastic constitutive basis, and some versions are amenable to computer implementation based on simple extensions of so-called return-mapping algorithms of the infinitesimal plasticity theory [30]. Unfortunately, efforts to utilize this approach to study shear band bifurcation are limited. The unregularized strong discontinuity formulation of Armero and Garikipati [31] and the regularized strong discontinuity stability analyses of Larsson and co-workers [32,33] provide critical starting points. However, they arrived at two different localization criteria for strong discontinuity bifurcation in elastoplastic solids that have no semblance to each other, except in the perfectly plastic case. In this paper we show that the difference between the two localization criteria lies in the postulated change in the character of the constitutive response at the bifurcation point.

It is well known that predictions of shear bands as a bifurcation from homogeneous deformation are strongly dependent on the constitutive description of homogeneous deformation. Unfortunately, two-invariant plasticity models may be inadequate for predicting the bifurcation point. Holcomb and Rudnicki [34] used a two-invariant plasticity model to predict the localization properties of Tennessee marble. They

concluded that the model could not predict any localization in the axisymmetric case—they found the required critical hardening modulus to be so negative that the model prediction never softened enough to reach this value. In contrast, a post-test examination of the specimens revealed that localization in the form of faulting did occur in most of the specimens. This problem is not restricted to their plasticity model but is emblematic of other simplified constitutive hypotheses in general [35]. The absence of the third stress invariant may have contributed to the model's poor prediction of the bifurcation point. In this paper, we address this concern by using in some of the numerical examples a class of three-invariant plasticity models with smooth yield surfaces to predict the localization properties of elastoplastic solids in the presence of large deformation.

## 2. General formulation for shear band mode bifurcation

In this section we establish a general framework for finite deformation bifurcation analysis of inelastic solids, focusing on the condition for the inception of a shear band in an initially homogeneously deforming continuum. The notations and symbols used throughout this paper are as follows: bold-face letters denote matrices and vectors; the symbol '·' denotes an inner product of two vectors (e.g. $\boldsymbol{a}\cdot\boldsymbol{b}=a_ib_i$), or a single contraction of adjacent indices of two tensors (e.g. $\boldsymbol{c}\cdot\boldsymbol{d}=c_{ij}d_{jk}$); the symbol ':' denotes an inner product of two second-order tensors (e.g. $\boldsymbol{c}:\boldsymbol{d}=c_{ij}d_{ij}$), or a double contraction of adjacent indices of tensors of rank two and higher (e.g. $\boldsymbol{C}:\boldsymbol{\epsilon}^{\mathrm{e}}=C_{ijkl}\epsilon^{\mathrm{e}}_{kl}$).

### 2.1. Shear band kinematics

Let $\phi:\mathscr{B}\to\mathscr{B}'$ be a $C^1$ configuration of $\mathscr{B}$ in $\mathscr{B}'$, where $\mathscr{B}$ and $\mathscr{B}'$ are general manifolds. The deformation gradient $\boldsymbol{F}$ is the tangent of $\phi$, $\boldsymbol{F}=T\phi$, so that for any material point $X$ in $\mathscr{B}$ we have the linear transformation $\boldsymbol{F}(X)$: $T_X\mathscr{B}\to T_{\phi(X)}\mathscr{B}'$. In coordinate form,

$$F_{aA}(X)=\frac{\partial\phi_a}{\partial X_A}(X)\Longleftrightarrow\boldsymbol{F}(X)=\frac{\partial\boldsymbol{\phi}}{\partial\boldsymbol{X}}(X). \tag{2.1}$$

We recall the symmetric right and left Cauchy–Green deformation tensors, $\boldsymbol{C}$ and $\boldsymbol{b}$, respectively, from the relations

$$\boldsymbol{C}=\boldsymbol{F}^{\mathrm{t}}\cdot\boldsymbol{F},\qquad\boldsymbol{b}=\boldsymbol{F}\cdot\boldsymbol{F}^{\mathrm{t}}. \tag{2.2}$$

In addition, four stress tensors are commonly encountered in the literature and will be used extensively throughout this paper: the nonsymmetric tensor $\boldsymbol{P}=$ first Piola–Kirchhoff, and the symmetric tensors $\boldsymbol{\sigma}=$ Cauchy, $\boldsymbol{\tau}=$ Kirchhoff (true), and $\boldsymbol{S}=$ second Piola–Kirchhoff. They are related via the relationships

$$\boldsymbol{S}=\boldsymbol{F}^{-1}\cdot\boldsymbol{P}=\boldsymbol{F}^{-1}\cdot\boldsymbol{\tau}\cdot\boldsymbol{F}^{-\mathrm{t}}=J\boldsymbol{F}^{-1}\cdot\boldsymbol{\sigma}\cdot\boldsymbol{F}^{-\mathrm{t}}, \tag{2.3}$$

where $J=\det(\boldsymbol{F})$ is the Jacobian.

In the presence of a shear band the kinematics of the problem changes slightly, as shown in Fig. 1. Here, $\mathscr{B}\subset R^{n_{\mathrm{sd}}}$ represents the reference configuration of a body with smooth boundary $\partial\mathscr{B}$, and $\boldsymbol{X}$ represents the position vector of any material point $X$ in $\mathscr{B}$. Let us consider a smooth manifold $\mathscr{S}_0\subset\mathscr{B}$ and denote points in $\mathscr{S}_0$ by $\boldsymbol{Y}$ through the parameters $\xi^1$, $\xi^2$ so that

$$\mathscr{S}_0=\{\boldsymbol{Y}=\widehat{\boldsymbol{Y}}(\xi^1,\xi^2)|(\xi^1,\xi^2)\in\mathscr{B}\}, \tag{2.4}$$

where $\widehat{\boldsymbol{Y}}:\mathscr{B}\to R^{n_{\mathrm{sd}}}$ is a smooth global parameterization. Thus, the unit normal to $\mathscr{S}_0$ is

$$\boldsymbol{N}=\widehat{\boldsymbol{N}}(\xi^1,\xi^2)=\widehat{\boldsymbol{Y}}_{,1}\times\widehat{\boldsymbol{Y}}_{,2}/\|\widehat{\boldsymbol{Y}}_{,1}\times\widehat{\boldsymbol{Y}}_{,2}\|. \tag{2.5}$$

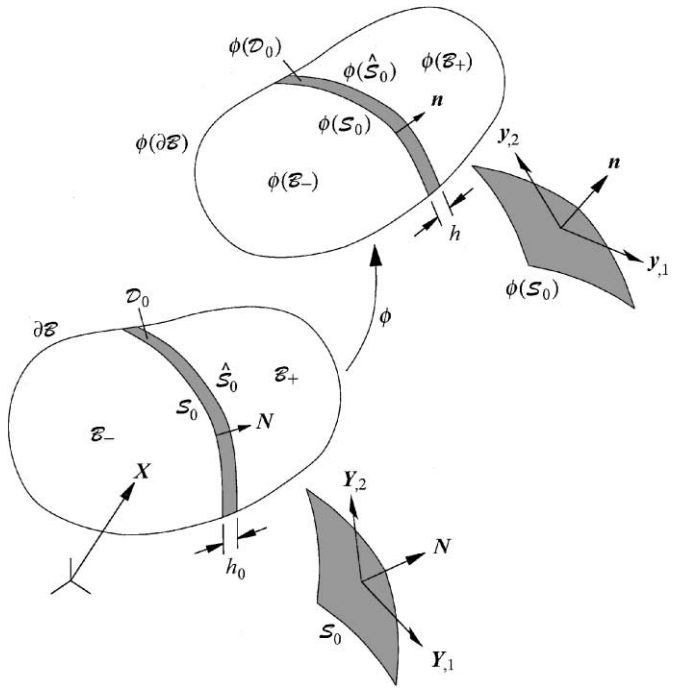


Fig. 1. Normal parameterization of shear band geometry with respect to reference and deformed configurations.

The above parameterization for $\mathscr{S}_0$ provides a convenient normal parameterization in the (closed) shear band domain $\overline{\mathscr{D}}_0 = \mathscr{S}_0 \times [0, h_0]$ so that any material position vector $\widehat{\boldsymbol{X}}$ in the shear band is defined by the mapping

$$\widehat{\boldsymbol{X}}(\xi^1, \xi^2, \kappa) = \widehat{\boldsymbol{Y}}(\xi^1, \xi^2) + \kappa \widehat{\boldsymbol{N}}(\xi^1, \xi^2) \qquad \text{for} \quad 0 \leqslant \kappa \leqslant h_0. \tag{2.6}$$

Thus, if we denote the curvilinear basis $\{\widehat{\boldsymbol{Y}}_{,1}, \widehat{\boldsymbol{Y}}_{,2}, \widehat{\boldsymbol{N}}\}$ associated with the normal parameterization, then the gradient of any function $f = f(\xi^1, \xi^2, \kappa)$ in $\overline{\mathscr{D}}_0$ is $(\partial f/\partial\kappa)\widehat{\boldsymbol{N}}$. In addition, a second smooth surface $\widehat{\mathscr{S}}_0$ is produced by the set relation

$$\widehat{\mathscr{S}}_0 = \{\boldsymbol{Y} = \widehat{\boldsymbol{X}}(\xi^1, \xi^2, h_0) | (\xi^1, \xi^2) \in \mathscr{B}\} \tag{2.7}$$

so that $\mathscr{S}_0$ and $\widehat{\mathscr{S}}_0$ are opposite surfaces representing the boundaries of the finite shear band as defined in the reference configuration. Throughout this paper, we will assume that the thickness parameter $h_0$ is small, and when $h_0 = 0$ then $\mathscr{S}_0 = \widehat{\mathscr{S}}_0$.

Next define the velocity field of any material point $X$ in $\mathscr{B}$ by the ramp-like relation

$$\boldsymbol{V}(X) = \begin{cases} \overline{\boldsymbol{V}} & \text{if } \kappa \leqslant 0; \\ \overline{\boldsymbol{V}} + \kappa[\![\boldsymbol{V}]\!]/h_0 & \text{if } 0 \leqslant \kappa \leqslant h_0; \\ \overline{\boldsymbol{V}} + [\![\boldsymbol{V}]\!] & \text{if } \kappa \geqslant h_0, \end{cases} \tag{2.8}$$

where $\overline{\boldsymbol{V}} = \overline{\boldsymbol{V}}(X)$ is a continuous velocity field, and $[\![\boldsymbol{V}]\!]$ represents the relative velocity of $\widehat{\mathscr{S}}_0$ to $\mathscr{S}_0$ induced by the shear band deformation, see Fig. 2. We recall that the material velocity $\boldsymbol{V}(X)$ of point $X$ is equal to the spatial velocity $\boldsymbol{v}(x)$ of point $x$ if the spatial point $x$ is the same material point $X$ in the reference configuration, i.e., $\boldsymbol{V}_t = \boldsymbol{v}_t \circ \phi_t$ for any time $t$. A similar remark may be made with respect to the relative velocity vector, i.e., $[\![\boldsymbol{V}]\!] = [\![\boldsymbol{v}]\!]$. Assuming $[\![\boldsymbol{V}]\!]$ is sufficiently uniform over $\widehat{\mathscr{S}}_0$, then the corresponding time derivatives of the deformation gradient tensor $\boldsymbol{F}$ outside and inside the shear band take the form

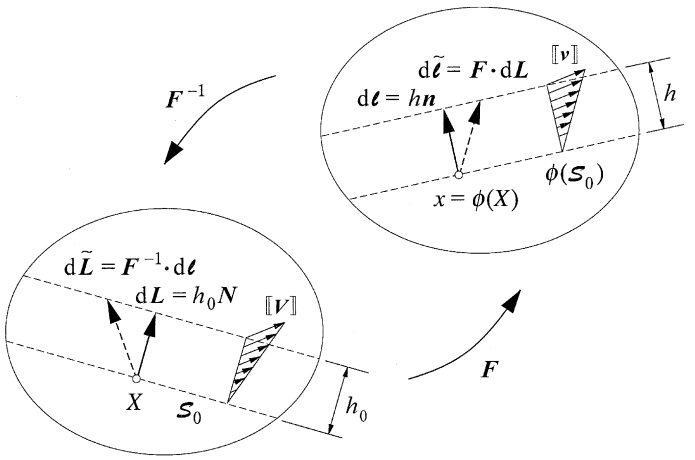


Fig. 2. Relative velocities and kinematics of motion of a material vector across a shear band.

$$\dot{\boldsymbol{F}} = \begin{cases} \dot{\overline{\boldsymbol{F}}} & \text{in } \mathscr{B} \setminus \overline{\mathscr{D}}_0; \\ \dot{\overline{\boldsymbol{F}}} + ([\![\boldsymbol{V}]\!] \otimes \boldsymbol{N})/h_0 & \text{in } \mathscr{D}_0, \end{cases} \tag{2.9}$$

where $\dot{\boldsymbol{F}} = \mathrm{GRAD}\boldsymbol{V}$, $\dot{\overline{\boldsymbol{F}}} = \mathrm{GRAD}\overline{\boldsymbol{V}}$, and $\mathscr{D}_0 = \mathscr{S}_0 \times (0, h_0)$ is the (open) shear band domain. Note that whereas $\dot{\boldsymbol{F}}$ is postulated to be possibly discontinuous on $\mathscr{S}_0$ (and $\widehat{\mathscr{S}}_0$), $\boldsymbol{F}$ is still smooth and continuous across the shear band before and at the moment of bifurcation. Evaluating just inside and just outside $\mathscr{S}_0$, we obtain the relation

$$\dot{\boldsymbol{F}}^1 = \dot{\boldsymbol{F}}^0 + \frac{1}{h_0}[\![\boldsymbol{V}]\!] \otimes \boldsymbol{N}. \tag{2.10}$$

Throughout this paper we will use the superscript symbols "1" and "0" to refer to points on $\mathscr{S}_0$ interpreted to lie just inside and just outside the band, respectively.

The results presented above may be used to derive expressions for the spatial velocity gradient inside and outside the shear band. Recalling the identity $\boldsymbol{l} = \dot{\boldsymbol{F}} \cdot \boldsymbol{F}^{-1}$, and noting that $\boldsymbol{F} \equiv \overline{\boldsymbol{F}}$ until the inception of localization, we obtain from (2.9)

$$\boldsymbol{l} = \begin{cases} \bar{\boldsymbol{l}} & \text{in } \phi(\mathscr{B}) \setminus \overline{\mathscr{D}}; \\ \bar{\boldsymbol{l}} + ([\![\boldsymbol{V}]\!] \otimes \boldsymbol{N} \cdot \boldsymbol{F}^{-1})/h_0 & \text{in } \mathscr{D}, \end{cases} \tag{2.11}$$

where $\bar{\boldsymbol{l}} = \dot{\overline{\boldsymbol{F}}} \cdot \boldsymbol{F}^{-1} = \dot{\overline{\boldsymbol{F}}} \cdot \overline{\boldsymbol{F}}^{-1}$ and $\mathscr{D} = \phi(\mathscr{D}_0)$.

The expression for the velocity gradient inside the shear band can be rewritten in spatial form by a similar reparameterization as follows. Consider the manifold $\mathscr{S} = \phi(\mathscr{S}_0)$ and denote points in $\mathscr{S}$ by $\boldsymbol{y}$ so that

$$\mathscr{S} = \{\boldsymbol{y} = \hat{\boldsymbol{y}}(\zeta^1, \zeta^2) | (\zeta^1, \zeta^2) \in \phi(\mathscr{B})\}, \tag{2.12}$$

where again, $\hat{\boldsymbol{y}} : \phi(\mathscr{B}) \to R^{n_{\mathrm{sd}}}$ is a smooth global parameterization. Thus, the unit normal to $\mathscr{S}$ is

$$\boldsymbol{n} = \hat{\boldsymbol{n}}(\zeta^1, \zeta^2) = \hat{\boldsymbol{y}}_{,1} \times \hat{\boldsymbol{y}}_{,2} / \|\hat{\boldsymbol{y}}_{,1} \times \hat{\boldsymbol{y}}_{,2}\|, \tag{2.13}$$

and so any point $\hat{\boldsymbol{x}}$ in the shear band is defined by the mapping

$$\hat{\boldsymbol{x}}(\zeta^1, \zeta^2, \kappa) = \hat{\boldsymbol{y}}(\zeta^1, \zeta^2) + \kappa \hat{\boldsymbol{n}}(\zeta^1, \zeta^2) \quad \text{for} \quad 0 \leqslant \kappa \leqslant h, \tag{2.14}$$

where the thickness parameter $h$ is again assumed to be small.

With this new normal parameterization the velocity field of any point $x$ in $\phi(\mathscr{B})$ may be defined by the ramp-like relation

$$\boldsymbol{v}(x) = \begin{cases} \bar{\boldsymbol{v}} & \text{if } \kappa \leqslant 0; \\ \bar{\boldsymbol{v}} + \kappa[\![\boldsymbol{v}]\!]/h & \text{if } 0 \leqslant \kappa \leqslant h; \\ \bar{\boldsymbol{v}} + [\![\boldsymbol{v}]\!] & \text{if } \kappa \geqslant h, \end{cases} \tag{2.15}$$

where $\bar{\boldsymbol{v}}_t = \boldsymbol{V}_t \circ \phi_t^{-1}$ is the inverse mapping of the velocity field. Thus, with respect to a new curvilinear basis $\{\hat{\boldsymbol{y}}_{,1}, \hat{\boldsymbol{y}}_{,2}, \hat{\boldsymbol{n}}\}$ associated with this new parameterization the velocity gradients may be determined directly as

$$\boldsymbol{l} = \begin{cases} \bar{\boldsymbol{l}} & \text{in } \phi(\mathscr{B}) \setminus \overline{\mathscr{D}}; \\ \bar{\boldsymbol{l}} + ([\![\boldsymbol{v}]\!] \otimes \boldsymbol{n})/h & \text{in } \mathscr{D}. \end{cases} \tag{2.16}$$

Evaluating just inside and just outside $\mathscr{S}$, we obtain the relation

$$\boldsymbol{l}^1 = \boldsymbol{l}^0 + \frac{1}{h}[\![\boldsymbol{v}]\!] \otimes \boldsymbol{n} \tag{2.17}$$

with superscripts "1" and "0" taking on the same meaning as before.

Comparing (2.11) and (2.16), we see that

$$\boldsymbol{N} \cdot \boldsymbol{F}^{-1}/h_0 = \boldsymbol{n}/h, \quad [\![\boldsymbol{V}]\!] = [\![\boldsymbol{v}]\!] \circ \phi. \tag{2.18}$$

This result has two geometric interpretations. First, take the scalar product of the first term of (2.18) with $\boldsymbol{n}$ and assume that $h$ is given. Thus, $\mathrm{d}\ell = h\boldsymbol{n}$ and a pull back to $\boldsymbol{X}$ gives

$$h_0 = \boldsymbol{N} \cdot \boldsymbol{F}^{-1} \cdot \mathrm{d}\ell = \boldsymbol{N} \cdot \mathrm{d}\widetilde{\boldsymbol{L}}. \tag{2.19}$$

Hence, $h_0$ is the normal projection of the elemental length $\mathrm{d}\widetilde{\boldsymbol{L}}$ to the surface $\mathscr{S}_0$. Now, assume that $h_0$ is given and let $\mathrm{d}\boldsymbol{L} = h_0\boldsymbol{N}$. A push forward to $\boldsymbol{x}$ gives

$$h = \boldsymbol{n} \cdot \boldsymbol{F} \cdot \mathrm{d}\boldsymbol{L} = \boldsymbol{n} \cdot \mathrm{d}\tilde{\ell}, \tag{2.20}$$

implying that $h$ is now the normal projection of the elemental length $\mathrm{d}\tilde{\ell}$ to $\mathscr{S}$. A pictorial representation of the shear band kinematics relating the operations indicated in (2.18)–(2.20) is shown in Fig. 2.

**Remark 1.** Nanson's formula states that $\boldsymbol{n}\,\mathrm{d}a = J\boldsymbol{F}^{-\mathrm{t}} \cdot \boldsymbol{N}\,\mathrm{d}A$, where $\mathrm{d}a$ and $\mathrm{d}A$ are infinitesimal surface areas whose unit normals are $\boldsymbol{n}$ and $N$, respectively, and $J$ is the jacobian [26]. Let $\mathrm{d}v = h\,\mathrm{d}a$, $\mathrm{d}V = h_0\,\mathrm{d}A$, and note that $J = \mathrm{d}v/\mathrm{d}V$ and $(\boldsymbol{F}^{-\mathrm{t}} \cdot \boldsymbol{N})_i = (\boldsymbol{N} \cdot \boldsymbol{F}^{-1})_i$. By inserting these into the above formula, one recovers the first term of (2.18).

In the limit of zero shear band thickness $[\![\boldsymbol{V}]\!]$ becomes a velocity jump discontinuity, and the velocity field takes the form

$$\boldsymbol{V} = \overline{\boldsymbol{V}} + [\![\boldsymbol{V}]\!]H_{\mathscr{S}}(X); \qquad H_{\mathscr{S}}(X) = \begin{cases} 1 & \text{if } X \in \mathscr{B}_+; \\ 0 & \text{if } X \in \mathscr{B}_-, \end{cases} \tag{2.21}$$

where $\overline{\boldsymbol{V}}$ is the continuous part of $\boldsymbol{V}$, $\mathscr{B}_+$ is the part of $\mathscr{B}$ in front of the band, and $\mathscr{B}_-$ is the part behind the band, see Fig. 1. In this case, theory of distribution may be used to express $\dot{\boldsymbol{F}}$ in the singular form

$$\dot{\boldsymbol{F}} = \begin{cases} \dot{\overline{\boldsymbol{F}}} & \text{in } \mathscr{B} \setminus \mathscr{S}_0; \\ \dot{\overline{\boldsymbol{F}}} + ([\![\boldsymbol{V}]\!] \otimes \boldsymbol{N})\delta_{\mathscr{S}} & \text{"in } \mathscr{S}_0\text{"}, \end{cases} \tag{2.22}$$

where quotes are used in the phrase "in $\mathscr{S}_0$" since the shear band volume actually vanishes in the limit. Thus,

$$\dot{\boldsymbol{F}}^1 = \dot{\boldsymbol{F}}^0 + (\llbracket \boldsymbol{V} \rrbracket \otimes \boldsymbol{N})\delta_{\mathscr{S}}, \tag{2.23}$$

where $\delta_{\mathscr{S}}$ is the Dirac delta symbol.

Similarly, in the limit of zero band thickness the velocity field can be defined as

$$\boldsymbol{v} = \bar{\boldsymbol{v}} + \llbracket \boldsymbol{v} \rrbracket H_{\mathscr{S}}(x); \quad H_{\mathscr{S}}(x) = \begin{cases} 1 & \text{if } x \in \phi(\mathscr{B}_+); \\ 0 & \text{if } x \in \phi(\mathscr{B}_-). \end{cases} \tag{2.24}$$

In this case the velocity gradient reduces to the form

$$\boldsymbol{l} = \begin{cases} \bar{\boldsymbol{l}} & \text{in } \phi(\mathscr{B}) \setminus \mathscr{S}; \\ \bar{\boldsymbol{l}} + (\llbracket \boldsymbol{v} \rrbracket \otimes \boldsymbol{n})\delta_{\mathscr{S}} & \text{"in } \mathscr{S}\text{"} \end{cases} \tag{2.25}$$

and

$$\boldsymbol{l}^1 = \boldsymbol{l}^0 + (\llbracket \boldsymbol{v} \rrbracket \otimes \boldsymbol{n})\delta_{\mathscr{S}}. \tag{2.26}$$

We shall refer to the limiting case $h = h_0 = 0$ as 'strong discontinuity' [35], as opposed to the case where $h$ and $h_0$ are small but finite which we shall refer to as 'weak discontinuity'.

### 2.2. Localization condition

For simplicity, attention will be restricted to the usual quasi-static problem focusing on the initiation of strain localization. In deriving the local equations of equilibrium for the problem at hand, our point of departure is the weak form of the linear momentum balance [36]

$$\mathscr{J}(\phi, \boldsymbol{\eta}) = \int_{\mathscr{B}} (\mathrm{GRAD}\,\boldsymbol{\eta} : \boldsymbol{P} - \rho_0 \boldsymbol{\eta} \cdot \boldsymbol{G})\,\mathrm{d}V - \int_{\partial\mathscr{B}^{\mathrm{t}}} \boldsymbol{\eta} \cdot \boldsymbol{t}\,\mathrm{d}A, \tag{2.27}$$

where $\rho_0 \boldsymbol{G}$ is the reference body force vector, $\boldsymbol{t} = \boldsymbol{P} \cdot \boldsymbol{v}$ is the *nominal* traction vector on $\partial\mathscr{B}^{\mathrm{t}} \subset \partial\mathscr{B}$, $\boldsymbol{v}$ is the unit vector on $\partial\mathscr{B}^{\mathrm{t}}$, and $\boldsymbol{\eta}$ is the weighting function. We assume the usual decomposition of boundaries, $\partial\mathscr{B}^{\mathrm{t}} \cup \partial\mathscr{B}^{\phi} = \partial\mathscr{B}$ and $\partial\mathscr{B}^{\mathrm{t}} \cap \partial\mathscr{B}^{\phi} = \emptyset$, where $\partial\mathscr{B}^{\phi}$ and $\partial\mathscr{B}^{\mathrm{t}}$ are the Dirichlet and Neumann boundaries, respectively.

In the presence of a shear band defined by the surface $\widetilde{\mathscr{S}}_0$, we can use integration by parts and Gauss theorem on the first term of $\mathscr{J}$ to obtain

$$\int_{\mathscr{B}\setminus\widetilde{\mathscr{S}}_0} \mathrm{GRAD}\,\boldsymbol{\eta} : \boldsymbol{P}\,\mathrm{d}V = -\int_{\mathscr{B}\setminus\widetilde{\mathscr{S}}_0} \boldsymbol{\eta} \cdot \mathrm{DIV}\boldsymbol{P}\,\mathrm{d}V + \int_{\widetilde{\mathscr{S}}_0} \boldsymbol{\eta} \cdot (\llbracket \boldsymbol{P} \cdot \boldsymbol{N} \rrbracket)\,\mathrm{d}A + \int_{\partial\mathscr{B}^{\mathrm{t}}} \boldsymbol{\eta} \cdot (\boldsymbol{P} \cdot \boldsymbol{v})\,\mathrm{d}A, \tag{2.28}$$

where $\boldsymbol{N}$ is the unit normal vector to $\widetilde{\mathscr{S}}_0$ and $\llbracket \boldsymbol{P} \cdot \boldsymbol{N} \rrbracket$ is a possible jump in the nominal traction vector across $\widetilde{\mathscr{S}}_0$. Inserting into (2.27) and setting $\mathscr{J}(\phi, \boldsymbol{\eta}) = 0$, a standard argument yields

$$\mathrm{DIV}\boldsymbol{P} + \rho_0 \boldsymbol{G} = \boldsymbol{0} \quad \text{in} \quad \mathscr{B} \setminus \widetilde{\mathscr{S}}_0; \tag{2.29a}$$

$$\boldsymbol{P} \cdot \boldsymbol{v} = \boldsymbol{t} \quad \text{on} \quad \partial\mathscr{B}^{\mathrm{t}}, \tag{2.29b}$$

supplemented with the condition

$$\llbracket \boldsymbol{P} \cdot \boldsymbol{N} \rrbracket = \llbracket \boldsymbol{P} \rrbracket \cdot \boldsymbol{N} = \boldsymbol{0} \quad \text{on} \quad \widetilde{\mathscr{S}}_0. \tag{2.30}$$

This suggests the suitability of the nominal traction vector $\boldsymbol{t}$ for shear band mode bifurcation analysis.

Let us now take the following linearization of $\mathscr{J}$ at configuration $\phi^\circ$

$$L\mathscr{J} = \mathscr{J}^\circ + \delta\mathscr{J}, \tag{2.31}$$

where $\delta\mathscr{J}$ is the usual variation of $\mathscr{J}$. Here, we investigate shear band mode bifurcation to possibly initiate at the configuration $\mathscr{J}^\circ$ and seek a critical direction, or set of directions, allowing such bifurcation to occur from among the bundle of possible variations $\delta\mathscr{J}$. For dead loading the variation of $\mathscr{J}$ takes the form

$$\delta\mathscr{J} = \int_{\mathscr{B}} \mathrm{GRAD}\,\boldsymbol{\eta} : \mathbf{A} : \delta\boldsymbol{F}\,\mathrm{d}V - \int_{\partial\mathscr{B}^{\mathrm{t}}} \boldsymbol{\eta}\cdot\delta\boldsymbol{t}\,\mathrm{d}A, \tag{2.32}$$

where $\delta\boldsymbol{F}$ is the variation of the deformation gradient tensor, $\delta\boldsymbol{t}$ is the variation of the nominal traction vector, and $\mathbf{A}$ is the first tangential moduli tensor defined explicitly by the relation

$$\delta\boldsymbol{P} = \mathbf{A} : \delta\boldsymbol{F}, \qquad \mathbf{A} = \frac{\partial\boldsymbol{P}}{\partial\boldsymbol{F}}, \qquad \mathsf{A}_{iAjB} = \frac{\partial P_{iA}}{\partial F_{jB}}. \tag{2.33}$$

In the presence of a shear band we can again use integration by parts and Gauss theorem on the first term of $\delta\mathscr{J}$ as before. Inserting the result into (2.32) and setting $\delta\mathscr{J} = 0$ yields the conditions

$$\mathrm{DIV}(\mathbf{A} : \delta\boldsymbol{F}) = \mathbf{0} \quad \text{in} \quad \mathscr{B}\setminus\widetilde{\mathscr{S}}_0; \tag{2.34a}$$

$$(\mathbf{A} : \delta\boldsymbol{F})\cdot\boldsymbol{v} = \delta\boldsymbol{t} \quad \text{on} \quad \partial\mathscr{B}^{\mathrm{t}}, \tag{2.34b}$$

supplemented with the condition

$$[\![\mathbf{A} : \delta\boldsymbol{F}]\!]\cdot\boldsymbol{N} = \mathbf{0} \quad \text{on} \quad \widetilde{\mathscr{S}}_0. \tag{2.35}$$

If the tangent operator $\mathbf{A}$ is continuous across the band, then (2.35) specializes to $(\mathbf{A} : [\![\delta\boldsymbol{F}]\!])\cdot\boldsymbol{N} = \mathbf{0}$ on $\widetilde{\mathscr{S}}_0$, where $[\![\delta\boldsymbol{F}]\!]$ is the jump in the variation of the deformation gradient. In this case, an equivalent expression for $\delta\boldsymbol{F}$ is facilitated by the rate $\dot{\boldsymbol{F}}$ itself, whose jump across the shear band is $[\![\dot{\boldsymbol{F}}]\!] = [\![\boldsymbol{V}]\!]\otimes\boldsymbol{N}/h_0$. Thus, for the case of a continuous $\mathbf{A}$, (2.35) results in the jump condition

$$\frac{1}{h_0}\boldsymbol{A}\cdot[\![\boldsymbol{V}]\!] = \mathbf{0}, \quad A_{ij} = N_A\mathsf{A}_{iAjB}N_B. \tag{2.36}$$

For $h_0 \neq 0$, nontrivial solutions to (2.36) exist if and only if

$$\det\boldsymbol{A} = 0. \tag{2.37}$$

Eq. (2.37) is a necessary condition for shear band mode bifurcation at finite strain and requires the initial vanishing of the determinant of so-called acoustic tensor $\boldsymbol{A}$ for some critical orientation $\boldsymbol{N}$. This particular form of the localization condition is the same as that presented by Bigoni [22]. Because $\boldsymbol{N}$ determines the critical unit normal vector in the reference configuration, we shall refer to $\boldsymbol{A}$ as the *Lagrangian acoustic tensor*.

In general, the constitutive operator $\mathbf{A}$ may depend on the mode of bifurcation and on the direction of the imposed deformation, particularly when the model is incrementally nonlinear. To overcome the difficulty associated with the possible nonlinearity of this constitutive operator, Hill [11] and Raniecki and Bruhns [37] proposed linear comparison solids which provide lower bound solutions to the range of possible bifurcations. For localization into a planar band mode the nonlinearity of the constitutive operator $\mathbf{A}$ arises from possible combinations of loading and unloading inside and outside the band, as well as on vertex effects [16,38]. As shown in [39,40], the latter effects naturally lead to a noncoaxiality between the principal stresses and principal plastic rates of deformation. In this paper we shall limit the discussion to conventional co-axial plasticity models where the principal directions of the stresses and the plastic rates of deformation coincide.

### 2.3. Strong discontinuity bifurcation

The limiting case $h = h_0 = 0$ has been termed 'strong discontinuity' in the literature [31–33,35,41–46], and has attracted much research attention lately because it facilitates a convenient finite element implementation within the framework of embedded discontinuity approaches. A peculiar feature of strong discontinuity kinematics is the development of a singular deformation gradient field as the shear band volume shrinks to zero. Bifurcation to such shear band mode requires appropriate interpretation of the localization criteria, heretofore based on the requirement that the nominal traction rate be continuous across the shear band, since strong discontinuity kinematics does not provide any finite volume "inside the band" on which to apply such traction continuity criterion.

The problem becomes more evident if one considers the traction jump condition for the regularized model,

$$\frac{1}{h_0}\boldsymbol{A}\cdot[\![\boldsymbol{V}]\!]=\boldsymbol{0}. \tag{2.38}$$

In an unregularized strongly discontinuous field $h_0 = 0$, and $[\![\boldsymbol{V}]\!]$ becomes a finite velocity jump. Clearly, nothing can be said of the nominal traction jump from (2.38), even if the determinant of $\boldsymbol{A}$ is forced to vanish, since strong discontinuity kinematics produces an indeterminate condition on the left-hand side that does not guarantee continuity of the nominal traction rate. A different interpretation of the localization condition is thus in order.

Consider the discontinuous velocity field (2.21) with corresponding time-derivatives of the deformation gradient, (2.22). At the moment of bifurcation the limiting nominal traction rate as $h_0 \to 0$ on any material point $X$ "inside the shear band" is

$$\dot{\boldsymbol{t}}^1(X)=\lim_{h_0\to 0}(\mathbf{A}:\dot{\boldsymbol{F}})\cdot\boldsymbol{N}|_X=(\mathbf{A}:\dot{\bar{\boldsymbol{F}}})\cdot\boldsymbol{N}|_X+[\mathbf{A}:([\![\boldsymbol{V}]\!]\otimes\boldsymbol{N})]\cdot\boldsymbol{N}|_X\delta_{\mathscr{S}}. \tag{2.39}$$

Now, in order for the nominal traction rate to be bounded, we must have

$$[\mathbf{A}:([\![\boldsymbol{V}]\!]\otimes\boldsymbol{N})]\cdot\boldsymbol{N}|_X=\boldsymbol{0}\Rightarrow\det\boldsymbol{A}(X)=0 \tag{2.40}$$

for some critical shear band orientation $\boldsymbol{N}$. Thus, in the strong discontinuity limit the determinant condition simply guarantees the boundedness of the nominal traction rate, and not necessarily the continuity of the traction rate across the band.

Because the shear band volume vanishes in the limit, it suffices to establish continuity of the nominal traction rates outside the two touching sides of the band, $\mathscr{S}_0=\widehat{\mathscr{S}}_0$, see definitions (2.4) and (2.7). To this end, let $X_+$ and $X_-$ denote material point $X$ interpreted as belonging to $\mathscr{B}_+$ and $\mathscr{B}_-$ on opposite sides of $\mathscr{S}_0$, respectively. The corresponding nominal traction rates are

$$\dot{\boldsymbol{t}}^0(X_+)=(\mathbf{A}:\dot{\bar{\boldsymbol{F}}})\cdot\boldsymbol{N}|_{X_+},\qquad \dot{\boldsymbol{t}}^0(X_-)=(\mathbf{A}:\dot{\bar{\boldsymbol{F}}})\cdot\boldsymbol{N}|_{X_-}. \tag{2.41}$$

Now, since $\mathbf{A}$, $\dot{\bar{\boldsymbol{F}}}$ and $\boldsymbol{N}$ are all continuous at point $X$, then $\dot{\boldsymbol{t}}^0(X_+)=\dot{\boldsymbol{t}}^0(X_-)=\dot{\boldsymbol{t}}^0(X)$, and the nominal traction rates on opposite sides of the band are continuous. As noted earlier, nothing can be said of the nominal traction rate "inside the band," $\dot{\boldsymbol{t}}^1(X)$, except that it is bounded, since the shear band volume vanishes in the limit. Thus, the localization criteria for $h \neq 0$ apply equally well to the limiting case $h = 0$ provided that the condition of traction continuity is interpreted in the above sense.

### 2.4. Tangent operators

The two-point tensor $\mathbf{A}$ can be related to other tangential moduli tensors used in nonlinear continuum mechanics. Here, we are interested in a rate constitutive equation relating the Kichhoff stress rate tensor to the spatial velocity gradient via the relation

$$\dot{\boldsymbol{\tau}}=\boldsymbol{\alpha}:\boldsymbol{l}, \tag{2.42}$$

where $\boldsymbol{\alpha}$ is a fourth-order spatial tangential moduli tensor. Denoting the tangential moduli $\mathsf{C}_{ABCD} = \partial S_{AB}/\partial C_{CD}$, where $C_{CD}$ is the component of the right Cauchy–Green deformation tensor $\boldsymbol{C}$, then we readily obtain the following analytical expression for $\boldsymbol{\alpha}$

$$\boldsymbol{\alpha} = \mathbf{c} + \boldsymbol{\tau} \oplus \mathbf{1} + \boldsymbol{\tau} \ominus \mathbf{1}, \qquad \mathsf{c}_{ijkl} = 2F_{iA}F_{jB}F_{kC}F_{lD}\mathsf{C}_{ABCD}, \tag{2.43}$$

where $(\boldsymbol{\tau} \oplus \mathbf{1})_{ijkl} = \tau_{jl}\delta_{ik}$ and $(\boldsymbol{\tau} \ominus \mathbf{1})_{ijkl} = \tau_{il}\delta_{jk}$. The above expression can readily be verified by substituting directly into (2.42) to obtain

$$\dot{\boldsymbol{\tau}} = \mathbf{c} : \boldsymbol{d} + \boldsymbol{l} \cdot \boldsymbol{\tau} + \boldsymbol{\tau} \cdot \boldsymbol{l}^{\mathrm{t}}, \tag{2.44}$$

where $\boldsymbol{d} = \mathrm{sym}(\boldsymbol{l})$ is the rate of deformation tensor, and $\mathbf{c} : \boldsymbol{d} \equiv \mathbf{c} : \boldsymbol{l}$ after noting the minor symmetry of $\mathbf{c}$ with respect to the indices $k$ and $l$, cf. Eq. (38.4) of [47].

Since $\boldsymbol{\tau} = \boldsymbol{P} \cdot \boldsymbol{F}^{\mathrm{t}}$, time differentiation gives

$$\dot{\boldsymbol{\tau}} = \boldsymbol{P} \cdot \dot{\boldsymbol{F}}^{\mathrm{t}} + \dot{\boldsymbol{P}} \cdot \boldsymbol{F}^{\mathrm{t}}. \tag{2.45}$$

The first term on the right-hand side yields

$$\boldsymbol{P} \cdot \dot{\boldsymbol{F}}^{\mathrm{t}} = \boldsymbol{P} \cdot (\boldsymbol{l} \cdot \boldsymbol{F})^{\mathrm{t}} = (\boldsymbol{\tau} \ominus \mathbf{1}) : \boldsymbol{l} \tag{2.46}$$

while the second term gives

$$\dot{\boldsymbol{P}} \cdot \boldsymbol{F}^{\mathrm{t}} = (\mathbf{A} : \dot{\boldsymbol{F}}) \cdot \boldsymbol{F}^{\mathrm{t}} = \mathbf{a} : \boldsymbol{l}. \tag{2.47}$$

We note that $\mathbf{a}$ is a spatial tangential moduli tensor obtained from the push-forward transformation

$$\mathsf{a}_{ikjl} = F_{kA}F_{lB}\mathsf{A}_{iAjB}. \tag{2.48}$$

Combining these results with (2.42) gives

$$\mathbf{a} = \boldsymbol{\alpha} - \boldsymbol{\tau} \ominus \mathbf{1} \tag{2.49}$$

from which the tensor $\mathbf{A}$ can be recovered from the pull-back transformation

$$\mathsf{A}_{iAjB} = F^{-1}_{Ak}F^{-1}_{Bl}\mathsf{a}_{ikjl}. \tag{2.50}$$

### 2.5. Alternative expression for localization condition

Substituting (2.50) into the expression for the Lagrangian acoustic tensor in the second term of (2.36) and using (2.18) gives

$$A_{ij} = N_A F^{-1}_{Ak}\mathsf{a}_{ikjl}N_B F^{-1}_{Bl} = \left(\frac{h_0}{h}\right)^2 n_k \mathsf{a}_{ikjl} n_l. \tag{2.51}$$

The jump condition (2.36) may then be written in the alternative form

$$\frac{h_0}{h^2}\boldsymbol{a} \cdot [\![\boldsymbol{v}]\!] = \mathbf{0}, \qquad a_{ij} = n_k \mathsf{a}_{ikjl} n_l. \tag{2.52}$$

For $h \neq 0$ and $h_0 \neq 0$, nontrivial solutions to (2.52) exist if and only if

$$\det \boldsymbol{a} = 0. \tag{2.53}$$

Eq. (2.53) provides an equivalent localization condition for the emergence of a shear band. Since the unit vector $\boldsymbol{n}$ is reckoned with respect to the current configuration, we shall refer to $\boldsymbol{a}$ as the *Eulerian acoustic tensor*.

**Remark 2.** The Lagrangian and Eulerian acoustic tensors are related by the expression

$$\boldsymbol{A} = \left(\frac{h_0}{h}\right)^2 \boldsymbol{a}. \tag{2.54}$$

The localization condition presented in [22] is based on the Lagrangian formulation and uses the same symbol $\boldsymbol{A}$ for the Lagrangian acoustic tensor. The localization condition described in [32,33] is based on the Eulerian formulation and uses the symbol $\boldsymbol{q}$ for the Eulerian acoustic tensor $\boldsymbol{a}$. Note from (2.54) that the vanishing of the determinants of the two acoustic tensors occurs at the same time, i.e., $\det \boldsymbol{a} = 0$ whenever $\det \boldsymbol{A} = 0$ and vice versa, yielding the critical shear band normals $\boldsymbol{N}$ and $\boldsymbol{n}$ that are either pull-back or push-forward of each other via Nanson's formula.

## 3. Bifurcation of elastoplastic solids

In this section we describe a finite deformation version of the infinitesimal plasticity theory. The formulation is based on multiplicative plasticity proposed in [48] and later developed extensively in [47]. A key aspect of the formulation is the development of an elastoplastic constitutive operator $\boldsymbol{\alpha}^{\mathrm{ep}}$ for use in the analysis of planar band bifurcation of elastoplastic solids.

### 3.1. Multiplicative plasticity in rate form

Following [44], we assume a multiplicative decomposition of the deformation gradient into elastic and plastic parts, $\boldsymbol{F} = \boldsymbol{F}^{\mathrm{e}} \cdot \boldsymbol{F}^{\mathrm{p}}$. As shown in [47], the Kirchhoff stress tensor $\boldsymbol{\tau}$ and the second Piola–Kirchhoff stress tensor $\overline{\boldsymbol{S}}$ are related from a thermodynamical principle by the equation

$$\boldsymbol{\tau} = \boldsymbol{F}^{\mathrm{e}} \cdot \overline{\boldsymbol{S}} \cdot \boldsymbol{F}^{\mathrm{et}}, \tag{3.1}$$

where the overline on $\overline{\boldsymbol{S}}$ denotes a description relative to the intermediate configuration, see Fig. 3. In terms of the elastic right Cauchy–Green deformation tensor $\boldsymbol{C}^{\mathrm{e}} = \boldsymbol{F}^{\mathrm{et}} \cdot \boldsymbol{F}^{\mathrm{e}}$, the tensor $\overline{\boldsymbol{S}}$ may be written for a hyperelastic material as $\overline{\boldsymbol{S}} = 2\partial\psi/\partial\boldsymbol{C}^{\mathrm{e}}$, where $\psi = \psi(\boldsymbol{C}^{\mathrm{e}})$ is the stored energy function [36].

Differentiating (3.1) with respect to time yields

$$\dot{\boldsymbol{\tau}} = \boldsymbol{\alpha}^{\mathrm{e}} : \boldsymbol{l}^{\mathrm{e}}, \tag{3.2}$$

where $\boldsymbol{l}^{\mathrm{e}} := \dot{\boldsymbol{F}}^{\mathrm{e}} \cdot \boldsymbol{F}^{\mathrm{e}-1}$ is the elastic component of the spatial velocity gradient,

$$\boldsymbol{\alpha}^{\mathrm{e}} = \mathbf{c}^{\mathrm{e}} + \boldsymbol{\tau} \oplus \mathbf{1} + \boldsymbol{\tau} \ominus \mathbf{1}, \qquad \mathrm{c}^{\mathrm{e}}_{ijkl} = 2F^{\mathrm{e}}_{iA}F^{\mathrm{e}}_{jB}F^{\mathrm{e}}_{kC}F^{\mathrm{e}}_{lD}\overline{\mathrm{C}}^{\mathrm{e}}_{ABCD} \tag{3.3}$$

and $\overline{\mathrm{C}}^{\mathrm{e}}_{ABCD} = \partial\overline{S}_{AB}/\partial C^{\mathrm{e}}_{CD}$. The velocity gradient $\boldsymbol{l} = \dot{\boldsymbol{F}} \cdot \boldsymbol{F}^{-1}$ follows from the multiplicative decomposition as [49]

$$\underbrace{\dot{\boldsymbol{F}} \cdot \boldsymbol{F}^{-1}}_{\boldsymbol{l}} = \underbrace{\dot{\boldsymbol{F}}^{\mathrm{e}} \cdot \boldsymbol{F}^{\mathrm{e}-1}}_{\boldsymbol{l}^{\mathrm{e}}} + \underbrace{\boldsymbol{F}^{\mathrm{e}} \cdot \dot{\boldsymbol{F}}^{\mathrm{p}} \cdot \boldsymbol{F}^{\mathrm{p}-1} \cdot \boldsymbol{F}^{\mathrm{e}-1}}_{\boldsymbol{l}^{\mathrm{p}}}. \tag{3.4}$$

Hence, (3.2) now becomes

$$\dot{\boldsymbol{\tau}} = \boldsymbol{\alpha}^{\mathrm{e}} : (\boldsymbol{l} - \boldsymbol{l}^{\mathrm{p}}). \tag{3.5}$$

We next assume a convex elastic domain $\boldsymbol{E}$ defined by a smooth yield surface $\mathscr{F}$ in stress space $\boldsymbol{\tau}$

$$\boldsymbol{E} = \{(\boldsymbol{\tau}, q) \in S \times R^{1+} | \mathscr{F}(\boldsymbol{\tau}, q) \leqslant 0\}, \tag{3.6}$$

where $S$ is the space of symmetric rank-two tensors and $q$ is a stress-like plastic internal variable describing the 'size' of the yield surface in Kirchhoff stress space. For the case of zero plastic spin (see [49] for a discussion of the relevance of the plastic spin) the antisymmetric part of $\boldsymbol{l}^{\mathrm{p}}$ vanishes, and so

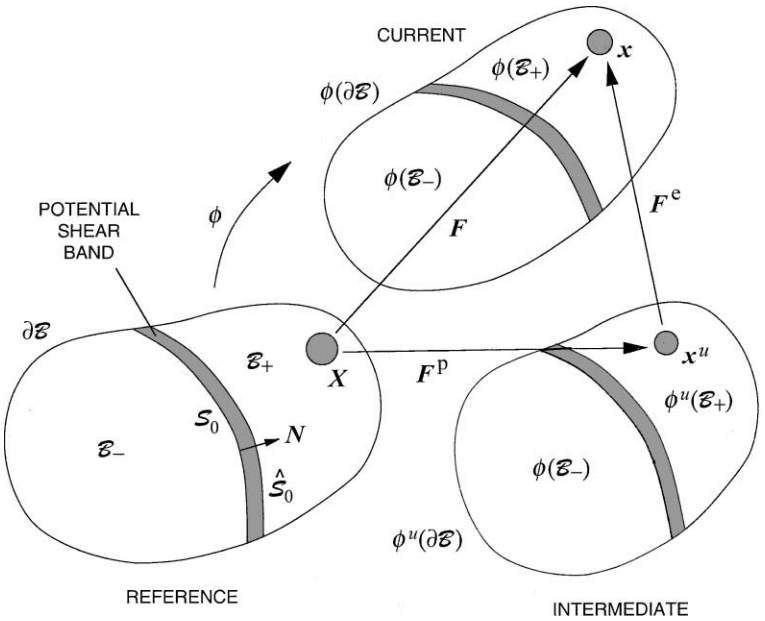


Fig. 3. Unloaded (or intermediate) configuration relative to reference and current configurations at onset of localization. Note: deformations are assumed to remain compatible up until the onset of localization.

$\boldsymbol{l}^p = \mathrm{sym}(\boldsymbol{l}^p) := \boldsymbol{d}^p$, where $\boldsymbol{d}^p$ is the plastic rate of deformation tensor. Assuming a smooth plastic potential function $\mathscr{Q}$ in the same Kirchhoff stress space, the flow rule writes

$$\boldsymbol{l}^p = \boldsymbol{d}^p = \dot{\lambda}\frac{\partial \mathscr{Q}}{\partial \boldsymbol{\tau}}, \tag{3.7}$$

where $\dot{\lambda}$ is a nonnegative plastic multiplier satisfying the Kuhn–Tucker complementarity conditions

$$\dot{\lambda} \geqslant 0, \qquad \mathscr{F}(\boldsymbol{\tau}, q) \leqslant 0, \qquad \dot{\lambda}\mathscr{F}(\boldsymbol{\tau}, q) = 0. \tag{3.8}$$

If $\mathscr{Q}$ is an isotropic function of stresses, then the principal stresses are coaxial with the principal plastic rates of deformation, leading to a so-called coaxial flow theory of plasticity [39,40].

We now proceed with the development of the elastoplastic constitutive model. For brevity we write the stress gradients as $\boldsymbol{f} = \partial\mathscr{F}/\partial\boldsymbol{\tau}$ and $\boldsymbol{q} = \partial\mathscr{Q}/\partial\boldsymbol{\tau}$. For plastic yielding the consistency condition writes

$$\dot{\mathscr{F}} = \boldsymbol{f} : \boldsymbol{\alpha}^e : (\boldsymbol{l} - \dot{\lambda}\boldsymbol{q}) - \dot{\lambda}\mathscr{H} = 0, \tag{3.9}$$

where $\mathscr{H}$ is the plastic modulus: hardening for $\mathscr{H} > 0$, softening for $\mathscr{H} < 0$, and perfect plasticity for $\mathscr{H} = 0$. Solving for the plastic multiplier gives

$$\dot{\lambda} = \frac{1}{\chi}\boldsymbol{f} : \boldsymbol{\alpha}^e : \boldsymbol{l}, \qquad \chi = \boldsymbol{f} : \boldsymbol{\alpha}^e : \boldsymbol{q} + \mathscr{H}. \tag{3.10}$$

Inserting the result into (3.5) yields

$$\dot{\boldsymbol{\tau}} = \boldsymbol{\alpha}^{ep} : \boldsymbol{l}, \tag{3.11}$$

where

$$\boldsymbol{\alpha}^{ep} = \boldsymbol{\alpha}^e - \boldsymbol{\alpha}^p, \qquad \boldsymbol{\alpha}^p = \frac{1}{\chi}\boldsymbol{\alpha}^e : \boldsymbol{q} \otimes \boldsymbol{f} : \boldsymbol{\alpha}^e \tag{3.12}$$

is the desired elastoplastic tangential moduli tensor. The above form of the rate constitutive equation is remarkably similar to that used in the infinitesimal theory.

**Remark 3.** If instead of $\psi = \psi(\boldsymbol{C}^{\mathrm{e}})$ we assume a stored energy function of the form $\widehat{\psi} = \widehat{\psi}(\boldsymbol{b}^{\mathrm{e}})$, where $\boldsymbol{b}^{\mathrm{e}} = \boldsymbol{F}^{\mathrm{e}} \cdot \boldsymbol{F}^{\mathrm{et}}$ is the elastic left Cauchy–Green deformation tensor, then the corresponding elastic constitutive equation is [30]

$$\boldsymbol{\tau} = 2\frac{\partial \widehat{\psi}}{\partial \boldsymbol{b}^{\mathrm{e}}} \cdot \boldsymbol{b}^{\mathrm{e}}.$$

Time differentiation of this equation gives

$$\dot{\boldsymbol{\tau}} = \tfrac{1}{2}\boldsymbol{\varphi} : \dot{\boldsymbol{b}}^{\mathrm{e}} \Longleftrightarrow \dot{\tau}_{ij} = \tfrac{1}{2}\varphi_{ijkl}\dot{b}^{\mathrm{e}}_{kl},$$

where $\boldsymbol{\varphi}$ is a rank-four tangential stress-deformation tensor with components

$$\varphi_{ijkl} = 2\left(\frac{\partial \widehat{\psi}}{b^{\mathrm{e}}_{il}}\delta_{jk} + \frac{\partial \widehat{\psi}}{\partial b^{\mathrm{e}}_{ik}}\delta_{jl}\right) + 4b^{\mathrm{e}}_{j\alpha}\frac{\partial^2 \widehat{\psi}}{\partial b^{\mathrm{e}}_{\alpha i}\partial b^{\mathrm{e}}_{kl}}.$$

Again, this leads to an elastic rate constitutive equation of the form (3.2), with

$$\alpha^{\mathrm{e}}_{ijkl} = \tau_{il}\delta_{jk} + 2\frac{\partial \widehat{\psi}}{\partial b^{\mathrm{e}}_{ik}}b^{\mathrm{e}}_{jl} + 4b^{\mathrm{e}}_{j\alpha}\frac{\partial^2 \widehat{\psi}}{\partial b^{\mathrm{e}}_{\alpha i}\partial b^{\mathrm{e}}_{k\beta}}b^{\mathrm{e}}_{\beta l}$$

as the elastic tangent constitutive tensor.

**Remark 4.** The Jaumann derivative of the Kirchhoff stress computed with the elastic spin tensor is given by

$$\overset{\nabla}{\tau} = \dot{\boldsymbol{\tau}} - \boldsymbol{w}^{\mathrm{e}} \cdot \boldsymbol{\tau} + \boldsymbol{\tau} \cdot \boldsymbol{w}^{\mathrm{e}}, \qquad \boldsymbol{w}^{\mathrm{e}} = \mathrm{skew}(\boldsymbol{l}^{\mathrm{e}}).$$

For isotropic yield function $\mathscr{F}$ with stress gradient $\boldsymbol{f} = \partial\mathscr{F}/\partial\boldsymbol{\tau}$, we get

$$\boldsymbol{f} : \dot{\boldsymbol{\tau}} = \boldsymbol{f} : \left(\overset{\nabla}{\boldsymbol{\tau}} + \boldsymbol{w}^{\mathrm{e}} \cdot \boldsymbol{\tau} - \boldsymbol{\tau} \cdot \boldsymbol{w}^{\mathrm{e}}\right) \equiv \boldsymbol{f} : \overset{\nabla}{\boldsymbol{\tau}}$$

since $\boldsymbol{f} : (\boldsymbol{\omega} \cdot \boldsymbol{\tau} - \boldsymbol{\tau} \cdot \boldsymbol{\omega}) = 0$ for any anti-symmetric tensor $\boldsymbol{\omega}$ [39]. The Jaumann derivative has been used artificially in the constitutive formulation of [31,47] leading to a slightly different form of the elastoplastic rate constitutive equation. However, as demonstrated above, the simplicity of the infinitesimal theory is easily recovered from the proposed formulation even without using the Jaumann derivative.

### *3.2. Constitutive formulation in the presence of a planar band*

To present the underlying idea more clearly we shall use the form (2.8) or (2.15) for the case of finite shear band thickness; the limiting case of zero band thickness is handled in a similar manner. Let us assume the following conditions to hold in the neighborhood of $\mathscr{S} = \phi(\mathscr{S}_0)$ at the onset of localization:

$$\boldsymbol{f} : \boldsymbol{\alpha}^{\mathrm{e}} : \left[\boldsymbol{l}^0 + \frac{1}{h}(\llbracket \boldsymbol{v} \rrbracket \otimes \boldsymbol{n})\right] > 0; \qquad \boldsymbol{f} : \boldsymbol{\alpha}^{\mathrm{e}} : \boldsymbol{l}^0 > 0, \tag{3.13}$$

where $\boldsymbol{l}^0 = \bar{\boldsymbol{l}}$ is the velocity gradient outside the band. This case describes the case of plastic yielding on both sides of the band at bifurcation [15,16].

Plastic loading implies that the true stress rate inside the band may be written in the form

$$\dot{\boldsymbol{\tau}}^{\mathrm{l}} = \boldsymbol{\alpha}^{\mathrm{e}} : \left[\bar{\boldsymbol{l}} + \frac{1}{h}(\llbracket \boldsymbol{v} \rrbracket \otimes \boldsymbol{n}) - \dot{\lambda}\boldsymbol{q}\right]. \tag{3.14}$$

Inserting into the consistency condition (3.9), we obtain

$$\dot{\mathscr{F}} = \boldsymbol{f} : \boldsymbol{\alpha}^{\mathrm{e}} : \left[\bar{\boldsymbol{l}} + \frac{1}{h}(\llbracket \boldsymbol{v} \rrbracket \otimes \boldsymbol{n}) - \dot{\lambda}\boldsymbol{q}\right] - \dot{\theta} = 0, \tag{3.15}$$

where $\dot{\lambda} > 0$ is the nonnegative plastic multiplier and $\dot{\theta} = \dot{\lambda}\mathscr{H}$ is the rate of hardening/softening of the yield function inside the band. We note that $\dot{\theta}$ and $\mathscr{H}$ have the same sign, and so

$$\dot{\theta} = \dot{\lambda}\mathscr{H} : \begin{cases} > 0 \Rightarrow \text{hardening;} \\ = 0 \Rightarrow \text{perfect plasticity;} \\ < 0 \Rightarrow \text{softening.} \end{cases} \tag{3.16}$$

It is important to recognize that the band thickness $h$ is typically many orders of magnitude smaller that the dimensions of the structure, and that we are dealing with a problem with two extreme scales. The multiscale nature of the problem is reflected in the form of the plastic multiplier $\dot{\lambda}$, which can be solved from (3.15) as

$$\dot{\lambda} = \dot{\bar{\lambda}} + \dot{\bar{\bar{\lambda}}}/h, \tag{3.17}$$

where $\dot{\bar{\lambda}}$ and $\dot{\bar{\bar{\lambda}}}$ are both regular functions given by

$$\dot{\bar{\lambda}} = \frac{1}{\chi}\boldsymbol{f} : \boldsymbol{\alpha}^{\mathrm{e}} : \bar{\boldsymbol{l}}, \qquad \dot{\bar{\bar{\lambda}}} = \frac{1}{\chi}\boldsymbol{f} : \boldsymbol{\alpha}^{\mathrm{e}} : (\llbracket \boldsymbol{v} \rrbracket \otimes \boldsymbol{n}) \tag{3.18}$$

and $\chi$ is given in (3.10). Thus, $\dot{\bar{\bar{\lambda}}}/h \gg \dot{\bar{\lambda}}$ for small $h$. Accordingly, the stress rate inside the band reflects the multiscale nature of the problem, and now takes the form

$$\dot{\boldsymbol{\tau}}^{\mathrm{l}} = \boldsymbol{\alpha}^{\mathrm{ep}} : \left[\bar{\boldsymbol{l}} + \frac{1}{h}(\llbracket \boldsymbol{v} \rrbracket \otimes \boldsymbol{n})\right] = \boldsymbol{\alpha}^{\mathrm{ep}} : \boldsymbol{l}^{\mathrm{l}}, \tag{3.19}$$

where $\boldsymbol{l}^{\mathrm{l}}$ is the velocity gradient inside the band and $\boldsymbol{\alpha}^{\mathrm{ep}}$ is the elastoplastic constitutive operator defined in (3.12). Since $\boldsymbol{\alpha}^{\mathrm{ep}}$ is continuous across the band, it may be used directly in (2.49) and in the subsequent developments of Section 2 leading to the relevant expressions for the elastoplastic acoustic tensors.

### 3.3. Stress rate at localization

The eigenvalue problem determines the unit normal vector $\boldsymbol{n}$ (or $\boldsymbol{N}$) to the band as well as the unit eigendirection $\llbracket \boldsymbol{v} \rrbracket / \|\llbracket \boldsymbol{v} \rrbracket\|$, but not the magnitude of the jump vector $\llbracket \boldsymbol{v} \rrbracket$ itself. Thus, at the onset of localization it is not possible to determine the stress rate $\dot{\boldsymbol{\tau}}^{\mathrm{l}}$ even if $h$ is prescribed in (3.19). However, it is possible to determine the character of $\dot{\boldsymbol{\tau}}^{\mathrm{l}}$ at bifurcation. This can be seen from the consistency condition at the bifurcation point,

$$\dot{\mathscr{F}} = \boldsymbol{f} : \dot{\boldsymbol{\tau}}^{\mathrm{l}} - \dot{\theta} = 0, \qquad \dot{\theta} = (\dot{\bar{\lambda}} + \dot{\bar{\bar{\lambda}}}/h)\mathscr{H}, \tag{3.20}$$

where $\mathscr{H} = \mathscr{H}_{\mathrm{cr}}$ at bifurcation. Since $\dot{\lambda} > 0$, it follows that: (a) if bifurcation occurs in the hardening regime ($\mathscr{H} > 0$), then $\boldsymbol{f} : \dot{\boldsymbol{\tau}}^{\mathrm{l}} > 0$ and the angle between $\boldsymbol{f}$ and $\dot{\boldsymbol{\tau}}^{\mathrm{l}}$ is acute; (b) if bifurcation occurs in the softening regime ($\mathscr{H} < 0$), then $\boldsymbol{f} : \dot{\boldsymbol{\tau}}^{\mathrm{l}} < 0$ and the angle between $\boldsymbol{f}$ and $\dot{\boldsymbol{\tau}}^{\mathrm{l}}$ is obtuse; and (c) for the case of perfect plasticity ($\mathscr{H} = 0$), then $\boldsymbol{f} : \dot{\boldsymbol{\tau}}^{\mathrm{l}} = 0$ and $\dot{\boldsymbol{\tau}}^{\mathrm{l}}$ is orthogonal to $\boldsymbol{f}$. More importantly, note that both $\boldsymbol{f}$ and $\mathscr{H}$ are regular functions, so for a vanishing $h$ both $|\dot{\theta}|$ and $\|\dot{\boldsymbol{\tau}}^{\mathrm{l}}\|$ *increase without bounds*.

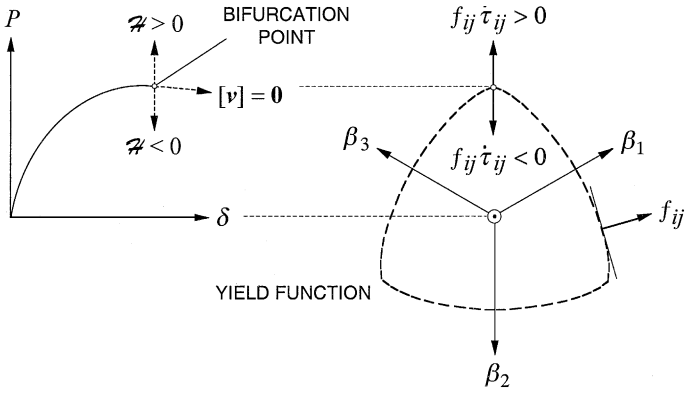


Fig. 4. Stress rates for vanishing band thickness $h$ in a uniaxial compression test. For bifurcation in the softening regime the instantaneous slope of the load-displacement curve is negative infinity; in the hardening regime the slope is positive infinity.

Fig. 4 shows the implications of (3.20) to localization in the context of a uniaxial compression test. Here, the axial load $P$ in the specimen is plotted as a function of the imposed boundary displacement $\delta$. At localization in the softening regime, and for a vanishing band thickness $h$, the instantaneous slope of the load-displacement curve bifurcates abruptly to negative infinity; for localization in the hardening regime the slope changes instantaneously to positive infinity. For the case of perfect plasticity, $\dot{\theta} = 0$, and the stress increment is theoretically constrained to lie on the fixed yield surface. Note that 'hardening' and 'softening' are defined herein based on the sign of $\mathscr{H}$ and not on the actual slope of the load-displacement response curve. The tangent to the 'homogeneous' load-displacement response curve at the bifurcation point corresponds to the trivial solution where $[\![\boldsymbol{v}]\!] = \mathbf{0}$.

The formation of a nearly vertical slope signifying rapid loss of strength due to strain localization (the case $\mathscr{H} < 0$ in Fig. 4) is backed up by experimental evidence. Holcomb and Rudnicki [34] inferred strain localization in Tennessee marble from the nearly vertical downward slope of the overall load-displacement curve exhibited by the specimen at some point in its load-displacement history (see Fig. 7 of [34]). If the plastic modulus $\mathscr{H}$ inside the band is to vary continuously with the imposed deformation, then any finite increment of imposed compression $\delta$ (no matter how small) would bring about a total loss of strength $P$; however, this is not always the case, and instead a gradual loss of strength at post-localization is commonly observed in practice. In order to capture the gradual loss of strength after bifurcation, the plastic modulus must thus change instantaneously to the form

$$\mathscr{H} \to \mathscr{H}_{\delta} h = \mathrm{O}(h), \tag{3.21}$$

where $\mathscr{H}_{\delta} < 0$ is a regular function, i.e., $\mathscr{H}$ must switch to a negative number of order $h$. In this case, the rate of change of the size of the yield function now becomes

$$\dot{\theta} = (\dot{\bar{\lambda}} + \dot{\bar{\bar{\lambda}}}/h)\mathscr{H}_{\delta} h = \dot{\bar{\lambda}}\mathscr{H}_{\delta} h + \dot{\bar{\bar{\lambda}}}\mathscr{H}_{\delta} \approx \dot{\bar{\bar{\lambda}}}\mathscr{H}_{\delta}, \tag{3.22}$$

which is a regular function, thus allowing the yield strength inside the band to decrease gradually. Note in (3.22) that the component $\dot{\bar{\lambda}}$ has no influence on $\dot{\theta}$ in the strong discontinuity limit.

### 3.4. Strong discontinuity in the hardening regime

On the other hand, infinite rates of stresses and hardening at the bifurcation point (the case $\mathscr{H} > 0$ in Fig. 4) are not observed in practice although their manifestation could have been obscured by an irregular

variation of the plastic modulus. The plastic modulus also could have switched character right at the moment of bifurcation preventing such infinite rates from ever occurring. A criterion for the onset of strong discontinuity in which the plastic modulus is assumed to take the form (3.21) right at the moment of bifurcation has gained acceptance in recent years [31,35,42–46,50]. As discussed below, this approach alters the final form of the localization condition.

Assume that at the moment of bifurcation the plastic modulus switches character as given in (3.21). The consistency condition inside the band then writes

$$\dot{\mathscr{F}} = \boldsymbol{f} : \boldsymbol{\alpha}^{\mathrm{e}} : \left[\bar{\boldsymbol{l}} + \frac{1}{h}([\![\boldsymbol{v}]\!] \otimes \boldsymbol{n}) - \dot{\lambda}\boldsymbol{q}\right] - \dot{\lambda}\mathscr{H}_{\delta} h = 0. \tag{3.23}$$

Solving for $\dot{\lambda} = \dot{\bar{\lambda}} + \dot{\bar{\bar{\lambda}}}/h$ yields

$$\dot{\bar{\lambda}} = \frac{1}{\widetilde{\chi}} \boldsymbol{f} : \boldsymbol{\alpha}^{\mathrm{e}} : \bar{\boldsymbol{l}}, \qquad \dot{\bar{\bar{\lambda}}} = \frac{1}{\widetilde{\chi}} \boldsymbol{f} : \boldsymbol{\alpha}^{\mathrm{e}} : ([\![\boldsymbol{v}]\!] \otimes \boldsymbol{n}), \tag{3.24}$$

where

$$\widetilde{\chi} = \boldsymbol{f} : \boldsymbol{\alpha}^{\mathrm{e}} : \boldsymbol{q} + \mathscr{H}_{\delta} h. \tag{3.25}$$

Note that $\widetilde{\chi} \to \boldsymbol{f} : \boldsymbol{\alpha}^{\mathrm{e}} : \boldsymbol{q}$ in the strong discontinuity limit. The stress rate now becomes

$$\dot{\boldsymbol{\tau}}^{1} = \widetilde{\boldsymbol{\alpha}}^{\mathrm{ep}} : \left[\bar{\boldsymbol{l}} + \frac{1}{h}([\![\boldsymbol{v}]\!] \otimes \boldsymbol{n})\right], \tag{3.26}$$

where

$$\widetilde{\boldsymbol{\alpha}}^{\mathrm{ep}} = \boldsymbol{\alpha}^{\mathrm{e}} - \frac{1}{\widetilde{\chi}} \boldsymbol{\alpha}^{\mathrm{e}} : \boldsymbol{q} \otimes \boldsymbol{f} : \boldsymbol{\alpha}^{\mathrm{e}}. \tag{3.27}$$

Going back to the consistency condition (3.23), we now write

$$\dot{\mathscr{F}} = \boldsymbol{f} : \dot{\boldsymbol{\tau}}^{1} - (\dot{\bar{\lambda}}\mathscr{H}_{\delta} h + \dot{\bar{\bar{\lambda}}}\mathscr{H}_{\delta}) = 0. \tag{3.28}$$

As $h \to 0$, $\dot{\theta} \to \dot{\bar{\bar{\lambda}}}\mathscr{H}_{\delta} =$ bounded, and so the stress rate inside the band remains bounded even in the strong discontinuity limit.

Since $\mathscr{H}$ inside the band is postulated to have switched character at bifurcation, the elastoplastic constitutive operator $\boldsymbol{\alpha}$ is no longer continuous across the band. Let $\widehat{\boldsymbol{\alpha}}$ be the constitutive operator outside the band relating the rate of the Kirchhoff stress to the corresponding velocity gradient, i.e.,

$$\dot{\boldsymbol{\tau}}^{0} = \widehat{\boldsymbol{\alpha}} : \bar{\boldsymbol{l}}. \tag{3.29}$$

Note that $\widehat{\boldsymbol{\alpha}} = \boldsymbol{\alpha}^{\mathrm{ep}}$ if the material outside the band is yielding plastically, and $\widehat{\boldsymbol{\alpha}} = \boldsymbol{\alpha}^{\mathrm{e}}$ if it is unloading elastically. From the chain rule, we obtain the time derivative of $\boldsymbol{P}^{0} = \boldsymbol{\tau}^{0} \cdot \boldsymbol{F}^{-\mathrm{t}}$ as

$$\dot{\boldsymbol{P}}^{0} = \widehat{\mathbf{A}} : \dot{\boldsymbol{F}}, \tag{3.30}$$

where $\widehat{\mathbf{A}}$ is the first tangential elasticity tensor evaluated just outside the band, with components

$$\widehat{\mathsf{A}}_{iAjB} = F^{-1}_{Ak} F^{-1}_{Bl} \widehat{\mathsf{a}}_{ikjl}, \qquad \widehat{\mathsf{a}}_{ikjl} = \widehat{\alpha}_{ikjl} - \tau^{0}_{il}\delta_{jk}. \tag{3.31}$$

Similarly, inside the band we have

$$\dot{\boldsymbol{P}}^{1} = \widetilde{\mathbf{A}}^{\mathrm{ep}} : \left[\dot{\boldsymbol{F}} + \frac{1}{h_0}([\![\dot{\boldsymbol{\phi}}]\!] \otimes \boldsymbol{N})\right], \tag{3.32}$$

where $\widetilde{\mathbf{A}}^{\mathrm{ep}}$ is the tangential moduli tensor with components

$$\widetilde{\mathsf{A}}^{\mathrm{ep}}_{iAjB} = F^{-1}_{Ak} F^{-1}_{Bl} \widetilde{\mathsf{a}}^{\mathrm{ep}}_{ikjl}, \qquad \widetilde{\mathsf{a}}^{\mathrm{ep}}_{ikjl} = \widetilde{\alpha}^{\mathrm{ep}}_{ikjl} - \tau^{1}_{il}\delta_{jk}. \tag{3.33}$$

The localization condition (2.30) now writes

$$(\dot{\boldsymbol{P}}^{1} - \dot{\boldsymbol{P}}^{0}) \cdot \boldsymbol{N} = \boldsymbol{0} \quad \text{on} \quad \widetilde{\mathscr{S}}_0 \tag{3.34}$$

or

$$[(\widetilde{\mathbf{A}}^{\mathrm{ep}} - \widehat{\mathbf{A}}) : \dot{\boldsymbol{F}}] \cdot \boldsymbol{N} + \frac{1}{h_0} \widetilde{\boldsymbol{A}} \cdot [\![\dot{\boldsymbol{\phi}}]\!] = \boldsymbol{0}, \qquad \widetilde{A}_{ij} = N_A \widetilde{\mathsf{A}}^{\mathrm{ep}}_{iAjB} N_B. \tag{3.35}$$

Note in this case that the localization condition depends on the band thickness $h_0$.

The limiting condition of strong discontinuity is of special interest since it allows the solution to continue beyond the bifurcation point using well-developed finite element enhancement procedures [31,35,42–46,50]. As $h_0 \to 0$ the first term in (3.35) remains a regular function while the second term increases without bounds. Thus, for the jump in the traction rate to remain bounded we must have

$$\widetilde{\boldsymbol{A}} \cdot [\![\dot{\boldsymbol{\phi}}]\!] = \boldsymbol{0} \Rightarrow \det(\widetilde{\boldsymbol{A}}) = 0, \tag{3.36}$$

where $\widetilde{\boldsymbol{A}}$ is now the limiting elastic-perfectly plastic acoustic tensor obtained by setting $h = 0$ in (3.25). Note that the above localization condition is true irrespective of whether the material outside the band is loading plastically or unloading elastically. A spatial counterpart of the localization condition may be derived by rewriting the jump condition (3.34) in the form (after skipping some details)

$$[(\widetilde{\mathbf{a}}^{\mathrm{ep}} - \widehat{\mathbf{a}}) : \bar{\boldsymbol{l}}] \cdot \boldsymbol{n} + \frac{1}{h} \widetilde{\boldsymbol{a}} \cdot [\![\dot{\boldsymbol{\phi}}]\!] = \boldsymbol{0}, \qquad \widetilde{a}_{ij} = n_k \widetilde{\mathbf{a}}^{\mathrm{ep}}_{ikjl} n_l. \tag{3.37}$$

Again, as $h \to 0$ the first term remains a regular function while the second term increases without bounds, unless we set

$$\widetilde{\boldsymbol{a}} \cdot [\![\dot{\boldsymbol{\phi}}]\!] = \boldsymbol{0} \Rightarrow \det(\widetilde{\boldsymbol{a}}) = 0. \tag{3.38}$$

The determinant condition is required for a nontrivial solution to exist.

Eqs. (3.36) and (3.38) are equivalent expressions describing condition for the onset of strong discontinuity localization. According to the consistency condition (3.28), the stress rate $\dot{\boldsymbol{\tau}}^{1}$ and the rate of hardening/softening of the yield surface $\dot{\theta}$ remain bounded as $h \to 0$. This condition is the same as that used in the unregularized strong discontinuity formulation of [31,35,42–46,50]. In reality it may be argued that the band thickness is always finite, in which case the localization condition based on a regularized strong discontinuity approach [14–16,33,41] may be used. However, we should recognize the fact that the difference in the scale still results in a very steep slope of the load-displacement response curve at localization. In [51] a procedure is adopted in which both the unregularized and the regularized localization conditions are checked and whichever comes first defines the strong discontinuity bifurcation point. Effectively, this procedure allows an accelerated softening response to occur at localization, but not an accelerated hardening response.

### 3.5. Elastoplastic constitutive operators in spectral form

Alternative analytical expressions may be developed for the elastoplastic constitutive operators $\boldsymbol{\alpha}^{\mathrm{ep}}$ and $\widetilde{\boldsymbol{\alpha}}^{\mathrm{ep}}$ compatible with the algorithmic calculations required by the finite deformation theory. The key is to write the Kirchhoff stress tensor in spectral form

$$\boldsymbol{\tau} = \sum_{A=1}^{3} \beta_A \boldsymbol{m}^{(A)}, \qquad \boldsymbol{m}^{(A)} = \boldsymbol{n}^{(A)} \otimes \boldsymbol{n}^{(A)}, \tag{3.39}$$

where $\boldsymbol{\beta} = \{\beta_1, \beta_2, \beta_3\}^{\mathrm{t}}$ are the principal values of $\boldsymbol{\tau}$, and the $\boldsymbol{n}^{(A)}$'s and $\boldsymbol{m}^{(A)}$'s are the corresponding eigendirections and eigenbases, respectively. Because of the assumed isotropy in the elastic response, the trial elastic left Cauchy–Green deformation tensor used in the product formula algorithm of multiplicative plasticity also takes the spectral form

$$\boldsymbol{b}^{\mathrm{e\,tr}} = \sum_{A=1}^{3} \gamma_A \boldsymbol{m}^{(A)}, \qquad \gamma_A = \lambda_A^2, \tag{3.40}$$

where the $\gamma_A$'s are the principal values of $\boldsymbol{b}^{\mathrm{e\,tr}}$ and the $\lambda_A$'s are the trial elastic principal stretches. We denote the principal elastic logarithmic strains as $\boldsymbol{\varepsilon}^{\mathrm{e}} = \{\varepsilon_1^{\mathrm{e}}, \varepsilon_2^{\mathrm{e}}, \varepsilon_3^{\mathrm{e}}\}^{\mathrm{t}}$, where $\varepsilon_A^{\mathrm{e}} = \ln(\lambda_A)$.

There are at least two ways of linearizing (3.39) to obtain the rate form $\dot{\boldsymbol{\tau}} = \boldsymbol{\alpha} : \boldsymbol{l}$. The first approach is to construct directly the principal values $\beta_A$ and the spectral directions (or eigenbases) $\boldsymbol{m}^{(A)}$, and then derive the tangential spin by closed-form linearization, see [30]. This approach does not require the evaluation of the individual eigenvectors $\boldsymbol{n}^{(A)}$, but the expression for the tangent operator $\boldsymbol{\alpha}$ is quite lengthy. The second approach is to extract the principal values $\beta_A$ and the eigenvectors $\boldsymbol{n}^{(A)}$, either in closed form or by numerical iteration, and utilize the spin of principal axes to develop an analytical expression for $\boldsymbol{\alpha}$ similar to that presented in [26]. The advantages and disadvantages of the two approaches are discussed in [52,53]. The two approaches theoretically lead to the same tangent operator $\boldsymbol{\alpha}$, and in this paper we shall use the second approach because it leads to a more compact expression [54,55],

$$\boldsymbol{\alpha} = \sum_{A=1}^{3}\sum_{B=1}^{3} a_{AB}\boldsymbol{m}^{(A)} \otimes \boldsymbol{m}^{(B)} + \sum_{A=1}^{3}\sum_{B\neq A} \frac{\beta_B - \beta_A}{\gamma_B - \gamma_A}\left(\gamma_B \boldsymbol{m}^{(AB)} \otimes \boldsymbol{m}^{(AB)} + \gamma_A \boldsymbol{m}^{(AB)} \otimes \boldsymbol{m}^{(BA)}\right), \tag{3.41}$$

where $a_{AB} = \partial\beta_A/\partial\varepsilon_B$ and $\boldsymbol{m}^{(AB)} = \boldsymbol{n}^{(A)} \otimes \boldsymbol{n}^{(B)}$.

The tangent operator $\boldsymbol{\alpha}$ is 'algorithmic' in the sense that it is used in conjunction with Newton iteration to advance the solution in discrete load increments, and thus reflects the nature of the algorithm used. Our goal is to construct the constitutive operators $\boldsymbol{\alpha}^{\mathrm{ep}}$ and $\widetilde{\boldsymbol{\alpha}}^{\mathrm{ep}}$ devoid of the effect of the numerical algorithm from the above algorithmic tangent operator. The elastoplastic constitutive operator is the limit

$$\boldsymbol{\alpha}^{\mathrm{ep}} = \lim_{\boldsymbol{b}^{\mathrm{e\,tr}} \to \boldsymbol{b}^{\mathrm{e}}} \boldsymbol{\alpha}, \tag{3.42}$$

where $\boldsymbol{b}^{\mathrm{e}} = \boldsymbol{F}^{\mathrm{e}} \cdot \boldsymbol{F}^{\mathrm{et}}$ is the current (converged) elastic left Cauchy–Green deformation tensor. Note that $\beta_A$, $\gamma_A$ and $\boldsymbol{n}^{(A)}$ are already being evaluated at each iteration, and thus do not have to be re-calculated, thereby motivating the aforementioned goal. The continuum limit of $a_{AB}$ is the elastoplastic constitutive matrix in principal axes,

$$a_{AB}^{\mathrm{ep}} = a_{AB}^{\mathrm{e}} - \frac{1}{X}\left(\sum_{I=1}^{3} a_{AI}^{\mathrm{e}} \frac{\partial \mathscr{Q}}{\partial \beta_I}\right)\left(\sum_{J=1}^{3} \frac{\partial \mathscr{F}}{\partial \beta_J} a_{JB}^{\mathrm{e}}\right), \tag{3.43}$$

where

$$X = \sum_{I=1}^{3}\sum_{J=1}^{3} \frac{\partial \mathscr{F}}{\partial \beta_I} a_{IJ}^{\mathrm{e}} \frac{\partial \mathscr{Q}}{\partial \beta_J} + \mathscr{H} \tag{3.44}$$

and $a_{IJ}^{\mathrm{e}}$ is the Hessian elastic matrix given in the next section. As noted earlier, the iterative solution already calculates the algorithmic tangent operator $\boldsymbol{\alpha}$ at each iteration; thus one only needs to replace the algorithmic tangent matrix $a_{AB}$ by the elastoplastic constitutive matrix $a_{AB}^{\mathrm{ep}}$ to form the constitutive operator $\boldsymbol{\alpha}^{\mathrm{ep}}$. The elastic-perfectly plastic constitutive operator $\widetilde{\boldsymbol{\alpha}}^{\mathrm{ep}}$ can be constructed using the same procedure but with $\mathscr{H}$ set to zero. Thus, the constitutive operators $\boldsymbol{\alpha}^{\mathrm{ep}}$ and $\widetilde{\boldsymbol{\alpha}}^{\mathrm{ep}}$ do not have to be re-constructed completely but may simply be derived from information that the iterative solution already provides.

## 4. Finite strain localization of dilatant frictional materials

### 4.1. Preliminaries

In this section we present three plasticity models used in the bifurcation analyses. We recall the stress invariants of the Kirchhoff stress tensor,

$$I_1 = \beta_1 + \beta_2 + \beta_3, \qquad I_2 = \beta_1\beta_2 + \beta_2\beta_3 + \beta_1\beta_3, \qquad I_3 = \beta_1\beta_2\beta_3. \tag{4.1}$$

In addition, the following stress invariant (not independent of the above three) is also useful

$$J_2 = \frac{1}{6}\left[(\beta_1 - \beta_2)^2 + (\beta_2 - \beta_3)^2 + (\beta_1 - \beta_3)^2\right]. \tag{4.2}$$

We consider a free energy function of the form

$$\Psi = U(\boldsymbol{\varepsilon}^{\mathrm{e}}) + \Psi^{\mathrm{e}}(\xi), \tag{4.3}$$

where $U(\boldsymbol{\varepsilon}^{\mathrm{e}})$ is the stored energy function that is quadratic in the principal elastic logarithmic stretches,

$$U(\boldsymbol{\varepsilon}^{\mathrm{e}}) = \tfrac{1}{2}\lambda[\varepsilon_1^{\mathrm{e}} + \varepsilon_2^{\mathrm{e}} + \varepsilon_3^{\mathrm{e}}]^2 + \mu[(\varepsilon_1^{\mathrm{e}})^2 + (\varepsilon_2^{\mathrm{e}})^2 + (\varepsilon_3^{\mathrm{e}})^2], \tag{4.4}$$

$\lambda$ and $\mu$ are the Lamé parameters, and $\Psi^{\mathrm{p}}(\xi)$ is the energy contribution of the plastic variable $\xi$ that also has a quadratic form,

$$\psi^{\mathrm{p}}(\xi) = \tfrac{1}{2}\mathscr{H}\xi^2. \tag{4.5}$$

For simplicity, we assume that the Lamé parameters $\lambda$ and $\mu$, as well as the plastic modulus $\mathscr{H}$ are all constant.

The principal Kirchhoff stresses are linear functions of the elastic logarithmic stretches,

$$\beta_A = \frac{\partial U}{\partial \varepsilon_A^{\mathrm{e}}} = \lambda\,\mathrm{tr}(\boldsymbol{\varepsilon}) + 2\mu\varepsilon_A^{\mathrm{e}}, \tag{4.6}$$

where

$$\mathrm{tr}(\boldsymbol{\varepsilon}^{\mathrm{e}}) = \ln(\lambda_1\lambda_2\lambda_3) = \ln[\det(\boldsymbol{F}^{\mathrm{e}})] = \ln\sqrt{\det(\boldsymbol{b}^{\mathrm{e}})} = \ln(J^{\mathrm{e}}). \tag{4.7}$$

The Hessian matrix $a_{AB}^{\mathrm{e}} = \nabla_{AB}^2(U)$ takes the form

$$a_{AB}^{\mathrm{e}} = \begin{bmatrix} \lambda + 2\mu & \lambda & \lambda \\ \lambda & \lambda + 2\mu & \lambda \\ \lambda & \lambda & \lambda + 2\mu \end{bmatrix} \tag{4.8}$$

so that the principal Kirchhoff stresses can also be written as

$$\beta_A = \sum_{B=1}^{3} a_{AB}^{\mathrm{e}}\varepsilon_B^{\mathrm{e}}. \tag{4.9}$$

The Hessian matrix $a_{AB}^{\mathrm{e}}$ is used to construct the constitutive operators described in Section 3.5.

### 4.2. Plasticity models

Three plasticity models are considered in the following.

Model 1. Quadratic logarithmic Drucker–Prager model

A two-invariant nonassociated Drucker–Prager model in Kirchhoff stress space is given by the yield function [56]

$$\mathscr{F} = \sqrt{\frac{3}{2}}J_2 - \sqrt{3}[A - BI_1/3] = 0 \tag{4.10}$$

and plastic potential function

$$\mathscr{Q} = \sqrt{\frac{3}{2}}J_2 - \sqrt{3}[A - bI_1/3], \tag{4.11}$$

where $A \geqslant 0$ and $B \geqslant 0$ are cohesion-like and friction-like parameters of the yield function, and $b \geqslant 0$ is a parameter associated with the plastic dilatancy of the model. If we denote the stress-like plastic variable by $q := \sqrt{3}A$, then $\partial\mathscr{F}/\partial q = \partial\mathscr{Q}/\partial q = -1$, and the model is associative with respect to hardening; further, if $b = B$ then we have the case of associative plasticity.

Model 2. Quadratic logarithmic Lade–Duncan model

A yield surface in Kirchhoff stress space that is a function of the first and third stress invariants is given by Lade and Duncan [57] as

$$\mathscr{F} = (k_1 I_3)^{1/3} - I_1 = 0, \tag{4.12}$$

where $k_1 \geqslant 27$ is a plastic internal variable characterizing the friction angle of the material. The minimum value of $k_1 = 27$ corresponds to the yield surface degenerating to the hydrostatic axis. Clearly, the yield surface passes through the stress space origin describing a 'cohesionless' material. Nonassociativity is invoked by taking a plastic potential function of the form

$$\mathscr{Q} = (k_2 I_3)^{1/3} - I_1, \tag{4.13}$$

where $k_2$ reflects the material's plastic dilatational response. The inequality $k_2 < k_1$ ensures a positive plastic dissipation [5]. Lade and Duncan originally formulated the model allowing for $k_1$ and $k_2$ to vary with plastic work. Here, however, we assume that these parameters are constant (perfect plasticity) so that the free-energy function (4.3) remains valid. A more realistic formulation of the model is possible, see [55].

Model 3. Quadratic logarithmic Matsuoka–Nakai model

A yield surface in Kirchhoff stress space that is a function of all three stress invariants is given by Matsuoka and Nakai [58] as

$$\mathscr{F} = (\bar{k}_1 I_3)^{1/3} - (I_1 I_2)^{1/3} = 0, \tag{4.14}$$

where $\bar{k}_1 \geqslant 9$ is a plastic internal variable similar in meaning to the parameter $k_1$ of the Lade–Duncan model. The minimum value of $\bar{k}_1 = 9$ corresponds to the yield surface coinciding with the hydrostatic axis. The yield surface also passes through the stress space origin, and thus characterizes a cohesionless material. A similar plastic potential function may be postulated,

$$\mathscr{Q} = (\bar{k}_2 I_3)^{1/3} - (I_1 I_2)^{1/3}, \tag{4.15}$$

where $\bar{k}_2 < \bar{k}_1$. For simplicity, we also assume in the analysis that $\bar{k}_1$ and $\bar{k}_2$ are constant (perfect plasticity).

Fig. 5 compares the three yield surfaces on the octahedral plane relative to the Mohr–Coulomb yield surface. Both the Drucker–Prager and Lade–Duncan yield surfaces can be made to pass through either the compression or tension corners of the Mohr–Coulomb surface, but not through all six corners. On the other hand, the three-invariant Matsuoka–Nakai model passes through all six corners of the Mohr–Coulomb surface. As required by the dilatant and frictional nature of the material, all yield surfaces define a cone that opens outward toward the negative hydrostatic axis. Analytical relationships among the

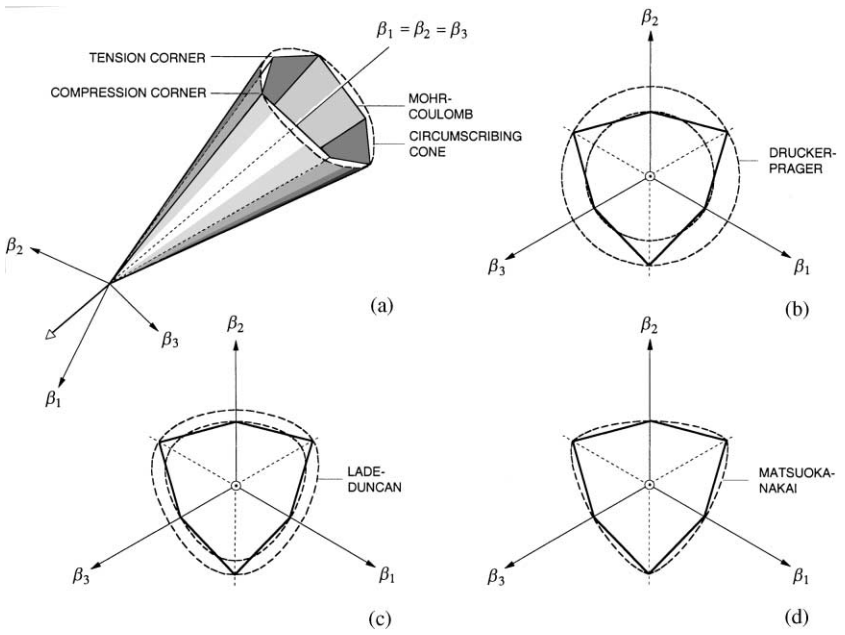


Fig. 5. Plasticity models: (a) Mohr–Coulomb yield surface in principal Kirchhoff stress space; (b) Drucker–Prager representation on octahedral plane; (c) Lade–Duncan; and (d) Matsuoka–Nakai yield surfaces (viewed from positive hydrostatic axis).

Lade–Duncan parameter $k_1$, the Matsuoka–Nakai parameter $\bar{k}_1$, and the Mohr–Coulomb friction angle parameter $\phi$ are available, see [54,55]. The stress-point integration algorithm is based on a product formula that utilizes a return mapping in principal Kirchoff stress space [30]; the derivatives of the three-invariant constitutive models are all given in [54,55].

### 4.3. Plane strain simulations

For plane strain condition on the plane $(x_1, x_2)$ the unit normal vector to the shear band reduces to the form $\boldsymbol{n} = \{n_1, n_2, 0\}$. Taking $n_1 = \cos\theta$ and $n_2 = \sin\theta$, where $\theta$ is the angle that the vector $\boldsymbol{n}$ makes with respect to the $x_1$-axis, the determinant of the Eulerian acoustic tensor becomes

$$\det(\boldsymbol{a}) = a_{11}a_{22} - a_{12}a_{21}. \tag{4.16}$$

This determinant function is plotted versus the angle $\theta$ to detect the onset of strain localization.

A specific example concerns the vertical compression of a rectangular specimen of dilatant frictional material. For analysis purposes the finite element mesh is shown in Fig. 6 and consists of 150 constant strain triangles. The level of mesh refinement is not an issue here since the state of stress is homogeneous before and until the moment of bifurcation. Vertical compression is prescribed through the top nodes, and the initial vanishing of the determinant is examined with increasing nominal vertical strain, $\Delta L/L_0$. For the record, the mesh is 1 m wide and 3 m tall ($L_0 = 3$ m). The following material parameters were held constant throughout the simulations: Drucker–Prager parameter $A = 17$ kPa, Poisson's ratio $v = 0.40$. The remaining parameters were varied as indicated in the figures.

Results of the localization analysis with the Drucker–Prager model are summarized in Figs. 7–11, where the determinant functions are plotted versus the angle $\theta$ at first localization. In each figure are plotted four determinant functions, two for large strain calculations and two for small strain, where each set of calculations examined the vanishing of the determinant of both the elastoplastic and the elastic-perfectly

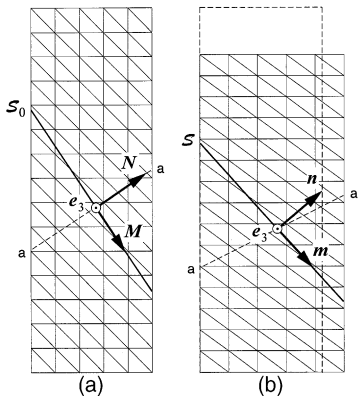


Fig. 6. Finite element mesh for plane strain compression simulations showing potential shear band orientations: (a) reference configuration; (b) current configuration.

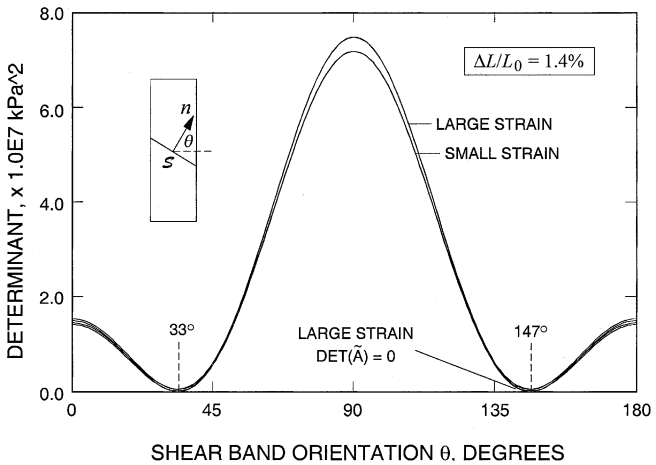


Fig. 7. Determinant function versus shear band orientation for plane strain compression problem, Drucker–Prager model: $E = 10,000$ kPa; $\mathscr{H}/E = 0.01$; $B = 0.495$; $b = 0.300$. Small strain formulation bifurcated at $\Delta L/L_0 = 1.5\%$.

plastic acoustic tensors. Nominal vertical strains at first localization are indicated in the box inserted in each figure. Note in all cases that localization is predicted sooner by the finite deformation model.

The general trend is as follows. Where the plastic modulus is positive (hardening), the vanishing of the determinant of the elastic-perfectly plastic acoustic tensor comes first; where the plastic modulus is negative (softening), the determinant of the elastoplastic acoustic tensor comes first. The discrepancy between the small and finite deformation bifurcation analyses is magnified at larger strains; for example, a nominal vertical strain of 12.7% is necessary for the finite deformation model to predict bifurcation in Fig. 10, whereas the small strain model required a much larger nominal vertical strain of 33% to initiate localization. An extreme case is shown in Fig. 11 where the finite deformation model predicted bifurcation for the case of hardening plasticity with associative plastic flow, whereas bifurcation is not possible with the infinitesimal formulation.

Figs. 12–14 show plots of the determinant function versus the angle $\theta$ using the three-invariant plasticity models of Lade–Duncan and Matsuoka–Nakai (note that the Lade–Duncan model may also be written in

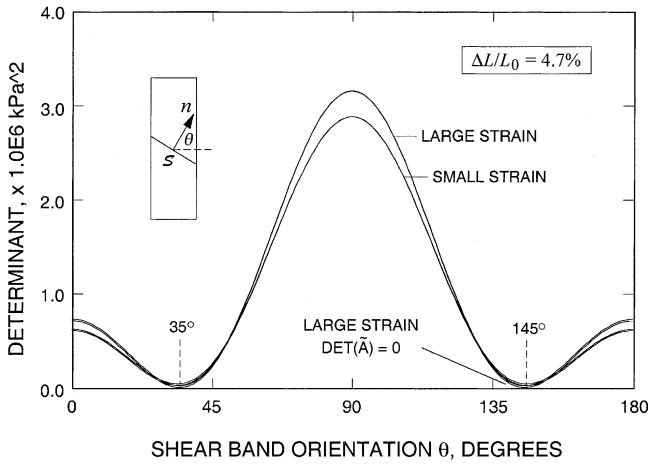


Fig. 8. Determinant function versus shear band orientation for plane strain compression problem, Drucker–Prager model: $E = 2000$ kPa; $\mathscr{H}/E = 0.01$; $B = 0.495$; $b = 0.300$. Small strain formulation bifurcated at $\Delta L/L_0 = 7.4\%$.

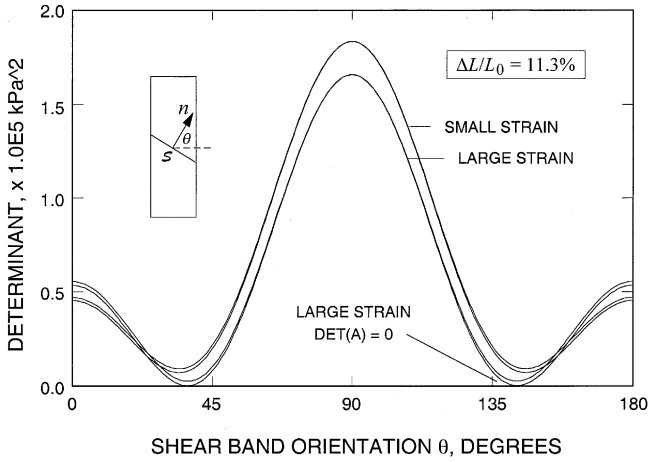


Fig. 9. Determinant function versus shear band orientation for plane strain compression problem, Drucker–Prager model: $E = 500$ kPa; $\mathscr{H}/E = -0.02$; $B = 0.495$; $b = 0.300$. Small strain formulation bifurcated at $\Delta L/L_0 = 23.0\%$.

terms of all three stress invariants, making it a three-invariant plasticity model as well, see [57]). The elastic constants were assumed as $E = 2000$ kPa and $v = 0.30$. Because the models are applicable to cohesionless materials such as sand, it was necessary to put the material under a confining pressure first before applying the vertical compression, and in the simulations we used a confining pressure of 67 kPa. Assuming a friction angle of 30°, we calculated the Lade–Duncan parameters as $k_1 = 38.11$ for yield surface passing through the tension corners of the Mohr–Coulomb yield surface, and $k_1 = 41.67$ for yield surface passing through the compression corners; for the Matsuoka–Nakai model, we calculated $\bar{k}_1 = 11.67$ for the same friction angle, see [54,55]. An associative flow rule was assumed in the simulations.

Results of the analyses also show the extreme case of bifurcation being predicted by the large deformation model when a small strain formulation would predict a stable plastic response throughout. The critical orientations of about 31° and 149° for the unit normal vector $\boldsymbol{n}$ indicate a shear band oriented at 59°

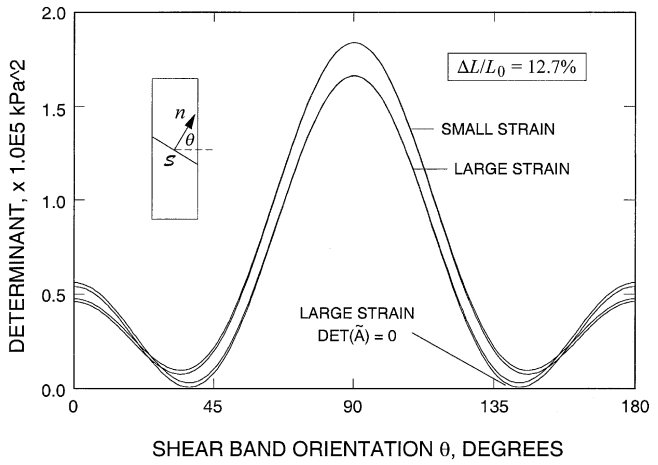


Fig. 10. Determinant function versus shear band orientation for plane strain compression problem, Drucker–Prager model: $E = 500$ kPa; $\mathscr{H}/E = 0.02$; $B = 0.495$; $b = 0.300$. Small strain formulation bifurcated at $\Delta L/L_0 = 33.0\%$.

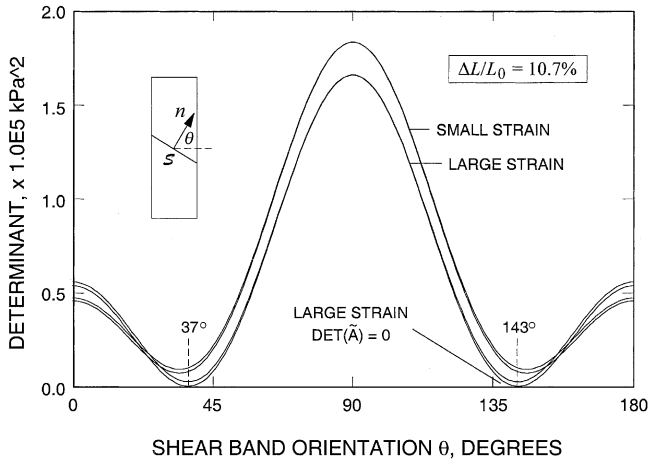


Fig. 11. Determinant function versus shear band orientation for plane strain compression problem, Drucker–Prager model: $E = 500$ kPa; $\mathscr{H}/E = 0.10$; $B = b = 0.300$. Small strain formulation did not bifurcate.

relative to the horizontal axis, which coincides with the axis of the minor principal compressive stress. This shear band orientation agrees with the expression $45° + \phi/2 = 60°$ commonly used in engineering practice, although it must be noted that the parameters $k_1$ and $\bar{k}_1$ were used in the simulations and not the value of the friction angle $\phi$. In further agreement with the analysis, the determinants of the elastoplastic and the elastic-perfectly plastic acoustic tensors vanish at the same time for the case of perfect plasticity.

**Remark 5.** Shear band orientations in the reference configuration may be obtained as follows. Consider the following finite element approximation for the deformation gradient in a typical finite element $\Omega^e$:

$$\boldsymbol{F} = \mathbf{1} + \frac{\partial \boldsymbol{u}}{\partial \boldsymbol{X}}, \qquad \boldsymbol{u} = \sum_{A=1}^{n_{\text{en}}} N_A \boldsymbol{d}_A^{\text{e}}, \qquad \boldsymbol{X} = \sum_{A=1}^{n_{\text{en}}} N_A \boldsymbol{X}_A^{\text{e}},$$

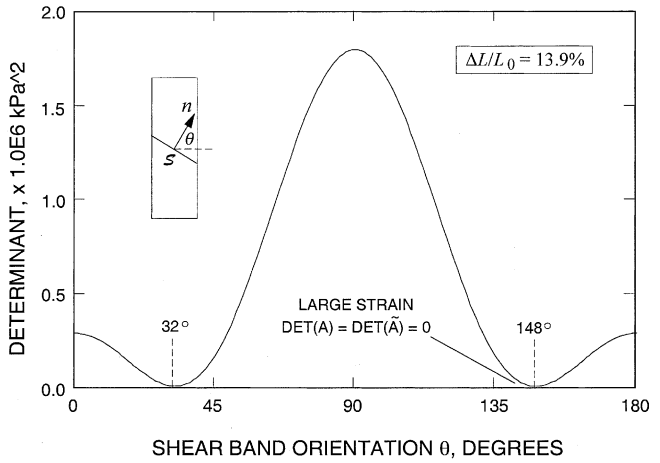


Fig. 12. Determinant function versus shear band orientation for plane strain compression problem, elastic-perfectly plastic Lade–Duncan model with associative flow rule: $E = 2000$ kPa; $v = 0.3$; $k_1 = 38.11$ ($\phi = 30°$ with yield surface passing through tension corners). Small strain formulation did not bifurcate.

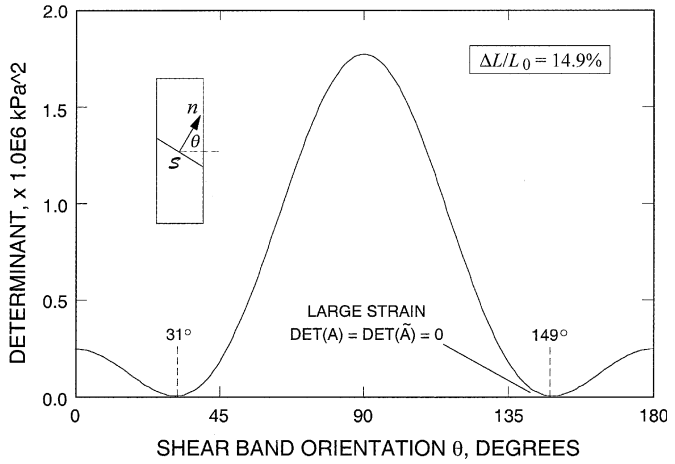


Fig. 13. Determination function versus shear band orientation for plane strain compression problem, elastic-perfectly plastic Lade–Duncan model with associative flow rule: $E = 2000$ kPa; $v = 0.3$; $k_1 = 41.67$ ($\phi = 30°$ with yield surface passing through compression corners). Small strain formulation did not bifurcate.

where $N_A$ are the element shape functions, $\boldsymbol{d}_A^{\mathrm{e}}$ are the element nodal displacements, $\boldsymbol{X}_A^{\mathrm{e}}$ are the element nodal reference coordinates, and $n_{\mathrm{en}}$ is the number of element nodes. Let $\boldsymbol{n}$ be the unit normal to $\mathscr{S}$ determined from the Eulerian acoustic tensor $\boldsymbol{a}$; then $\boldsymbol{m} = \boldsymbol{n} \times \boldsymbol{e}_3$ is the unit tangent to $\mathscr{S}$. The pull back $\boldsymbol{M} = \boldsymbol{F}^{-1} \cdot \boldsymbol{m}$ gives the tangent to $\mathscr{S}_0$ (not necessarily of unit length because of the stretching), and $\boldsymbol{N} = \boldsymbol{e}_3 \times \boldsymbol{M}/\|\boldsymbol{e}_3 \times \boldsymbol{M}\|$ describes the unit normal vector to $\mathscr{S}_0$. Clearly, the same vector $\boldsymbol{N}$ can be determined directly from the Lagrangian acoustic tensor $\boldsymbol{A}$. The pertinent vectors are shown in Fig. 6.

In summary, we can make the following conclusions based on the above results. The unregularized strong discontinuity bifurcation model of [31,35,42–46,50] prevents the stress rate and the rate of

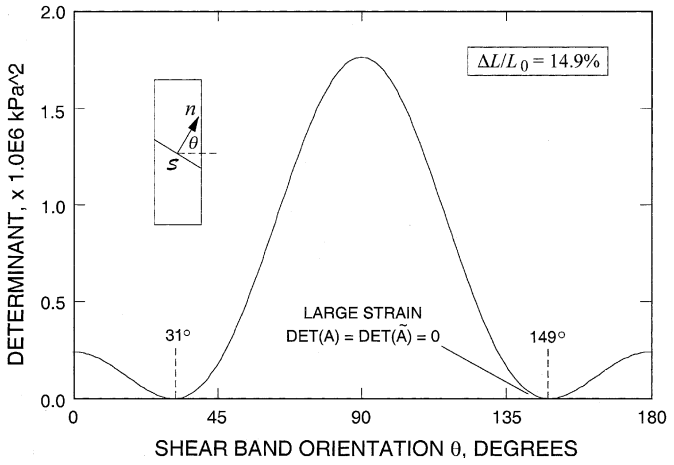


Fig. 14. Determinant function versus shear band orientation for plane strain compression problem, elastic-perfectly plastic Matsuoka–Nakai model with associative flow rule: $E = 2000$ kPa; $\nu = 0.3$; $\bar{k}_1 = 11.67$ ($\phi = 30°$). Small strain formulation did not bifurcate.

hardening/softening of the yield function to increase without bounds by postulating the plastic modulus to switch character at localization. However, this criterion is valid only in the limiting strong discontinuity case, and for a finite band thickness the complete localization condition that approaches this unregularized limit is given either by (3.35) or (3.37). On the other hand, the regularized strong discontinuity bifurcation model of [14–16,33,41] is valid only for a finite band thickness. In the unregularized limit this criterion predicts an infinite stress rate and an infinite rate of hardening/softening of the yield function except in the perfectly plastic case. Because of the difference in the character of the assumed constitutive response at the bifurcation point, the localization criteria predicted by the unregularized and the regularized models are different except in the special case of perfect plasticity.

## 5. Closure

The problem of shear band mode bifurcation of elastoplastic solids has been investigated incorporating geometric nonlinearities. Conditions for the onset of strain localization are based on the requirement of continuity of the nominal traction vector, and are described in the reference and deformed configurations by the vanishing of the determinant of the Lagrangian and Eulerian acoustic tensors. Results of the analysis show that finite deformation effects do enhance strain localization, and that bifurcation is possible even in the hardening regime of an associative plasticity model. This may be attributed to the additional stress terms that destroy the symmetry of the tangent operators even in the ideal case of associative plasticity.

Bifurcation analysis is a crucial step in strain localization modeling. In finite element analysis the bifurcation point identifies the critical stage of the solution at which the element interpolations may be enhanced to capture the post-localization response. Unfortunately, predictions of shear bands as a bifurcation from homogeneous deformation are strongly dependent on the constitutive description of homogeneous deformation. Although we have incorporated finite deformation effects and all three stress invariants in an attempt to improve on the kinematical and constitutive descriptions of the material/structural response, the present paper still deals only with co-axial flow theory of plasticity. Noncoaxial plastic flow induced, for example, by vertex yielding, and the incremental nonlinearity in the constitutive response remain two of the more intriguing aspects of the theory yet to be incorporated in routine strain localization analysis.

## Acknowledgements

The author is grateful to Claudio Tamagnini and Jacques Desrues for enlightening discussions pertaining to issues in bifurcation analysis; to Medji Sama and Victor Calo for reading and reviewing the initial drafts of the manuscript; and to anonymous reviewers for their constructive reviews. The work presented in this paper was supported in part by National Science Foundation through grant no. CMS97-00426.

## References

[1] A. Nádai, Plasticity, McGraw-Hill, New York, 1931.
[2] A. Aydin, Small faults formed as deformation bands in sandstone, PAGEOPH 116 (1978) 913–930.
[3] J.W. Hutchinson, K.W. Neale, Neck propagation, J. Mech. Phys. Solids 31 (1983) 405–426.
[4] H.E. Read, G.A. Hegemier, Strain softening of rock, soil and concrete—A review article, Mech. Mater. 3 (1984) 271–294.
[5] P.A. Vermeer, R. de Borst, Nonassociated plasticity for soils, concrete, and rock, Heron 29 (1984) 1–64.
[6] I. Vardoulakis, B. Graf, Calibration of constitutive models for granular materials using data from biaxial experiments, Géotechnique 35 (1985) 299–317.
[7] M.F. Ashby, S.D. Hallam, The failure of brittle solids containing small cracks under compressive stress states, Acta Metall. 16 (1986) 497–510.
[8] Z.P. Bazant, J. Planas, Fracture and Size Effect in Concrete and Other Quasibrittle Materials, CRC Press, Boca Raton, Florida, 1998.
[9] E. van der Giessen, R. de Borst, Introduction to material instabilities in solids, in: R. de Borst, E. van der Giessen (Eds.), Chapter 1: Material Instabilities in Solids, John Wiley, New York, 1998, pp. 1–13.
[10] J. Hadamard, Lecons sur la Propagation des Ondes, Herman et fil, Paris, 1903.
[11] R. Hill, A general theory of uniqueness and stability in elastic–plastic solids, J. Mech. Phys. Solids 6 (1958) 236–249.
[12] T.Y. Thomas, Plastic flow and fracture of solids, Academic Press, New York, 1961.
[13] J. Mandel, Conditions de stabilité et postulat de Drucker, In: Proceedings IUTAM Symposium on Rheology and Soil Mechanics, Springer-Verlag, Berlin, 1966, pp. 58–68.
[14] J.R. Rice, The localization of plastic deformation, in: W.T. Koiter (Ed.), Theoretical and Applied Mechanics, North-Holland Publishing Co., The Netherlands, 1976, pp. 207–220.
[15] J.W. Rudnicki, J.R. Rice, Conditions for the localization of deformation in pressure-sensitive dilatant materials, J. Mech. Phys. Solids 23 (1975) 371–394.
[16] J.R. Rice, J.W. Rudnicki, A note on some features of the theory of localization of deformation, Int. J. Solids Struct. 16 (1980) 597–605.
[17] D. Kolymbas, Bifurcation analysis for sand samples with a non-linear constitutive equation, Ingenieur-Archiv 50 (1981) 131–140.
[18] J. Desrues, R. Chambon, Shear band analysis for granular materials: the question of incremental non-linearity, Ingenieur-Archiv 59 (1989) 187–196.
[19] R. Chambon, S. Crochepeyre, J. Desrues, Localization criteria for non-linear constitutive equations of geomaterials, Mech. Cohes.-Frict. Mater. 5 (2000) 61–82.
[20] C. Tamagnini, G. Viggiani, R. Chambon, Some remarks on shear band analysis in hypoplasticity, in: H.-B. Mühlhaus, A. Dyskin, E. Pasternak (Eds.), Bifurcation and Localisation Theory in Geomechanics, Balkema, Lisse, 2001, pp. 85–93.
[21] R.W. Ogden, Local and global bifurcation phenomena in plane-strain finite elasticity, Int. J. Solids Struct. 21 (1985) 121–132.
[22] D. Bigoni, Bifurcation and instability of non-associative elastoplastic solids, CISM Lecture Notes on the Course: Material Instabilities in Elastic and Plastic Solids, H. Petryk (Coordinator), Udine, Sept. 13–17, 1999.
[23] J.C. Simo, T.J.R. Hughes, Computational Inelasticity, Springer, New York, 1998.
[24] R. Hill, On constitutive inequalities for simple materials, J. Mech. Phys. Solids 16 (1968) 229–242.
[25] R. Hill, J.R. Rice, Elastic potentials and the structure of inelastic constitutive laws, SIAM J. Appl. Math. 25 (1973) 448–461.
[26] R.W. Ogden, Non-linear Elastic Deformations, Chichester, Ellis Horwood Ltd., 1984.
[27] J. Mandel, Thermodynamics and plasticity, in: J.J. Delgado Domingers, N.R. Nina, J.H. Whitelaw (Eds.), Foundations of Continuum Thermodynamics, Macmillan, London, 1974, pp. 283–304.
[28] J.H. Argyris, J.St. Doltsinis, On the large strain inelastic analysis in natural formulation—Part I: Quasistatic problems, Comput. Methods Appl. Mech. Engrg. 20 (1979) 213–252.
[29] J.C. Simo, R.L. Taylor, Quasi-incompressible finite elasticity in principal stretches. Continuum basis and numerical algorithms, Comput. Methods Appl. Mech. Engrg. 85 (1991) 273–310.
[30] J.C. Simo, Algorithms for static and dynamic multiplicative plasticity that preserve the classical return mapping schemes of the infinitesimal theory, Comput. Methods Appl. Mech. Engrg. 99 (1992) 61–112.

[31] F. Armero, K. Garikipati, An analysis of strong discontinuities in multiplicative finite strain plasticity and their relation with the numerical simulation of strain localization in solids, Int. J. Solids Struct. 33 (1996) 2863–2885.
[32] R. Larsson, P. Steinmann, K. Runesson, Finite element embedded localization band for finite strain plasticity based on a regularized strong discontinuity, Mech. Cohes.-Frict. Mater. 4 (1998) 171–194.
[33] P. Steinmann, R. Larson, K. Runesson, On the localization properties of multiplicative hyperelasto-plastic continua with strong discontinuities, Int. J. Solids Struct. 34 (1997) 969–990.
[34] D.J. Holcomb, J.W. Rudnicki, Inelastic constitutive properties and shear localization in Tennessee marble, Int. J. Num. Anal. Meth. Geomech. 25 (2001) 109–129.
[35] J.C. Simo, J. Oliver, F. Armero, An analysis of strong discontinuities induced by strain-softening in rate-independent inelastic solids, Comput. Mech. 12 (1993) 277–296.
[36] J.E. Marsden, T.J.R. Hughes, Mathematical Foundations of Elasticity, Dover Publications, Inc., New York, 1983.
[37] B. Raniecki, O.T. Bruhns, Bounds to bifurcation stresses in solids with non-associated plastic flow law at finite strain, J. Mech. Phys. Solids 29 (1981) 153–171.
[38] S. Stören, J.R. Rice, Localized necking in thin sheets, J. Mech. Phys. Solids 23 (1975) 421–441.
[39] E. Papamichos, I. Vardoulakis, Shear band formation in sand according to non-coaxial plasticity model, Géotechnique 45 (1991) 649–661.
[40] J. Sulem, I. Vardoulakis, E. Papamichos, A. Oulahna, J. Tronvoll, Elasto-plastic modelling of Red Wildmoor sandstone, Mec. Cohes.-Frict. Mater. 4 (1999) 215–245.
[41] R. Larsson, K. Runesson, Discontinuous displacement approximation for capturing plastic localization, Int. J. Num. Methods Engrg. 36 (1993) 2087–2105.
[42] J.C. Simo, J. Oliver, A new approach to the analysis and simulation of strain softening in solids, in: Z.P. Bazant, et al. (Eds.), Fracture and Damage in Quasibrittle Structures, E.& F.N. Spon, London, 1994, pp. 25–39.
[43] F. Armero, K. Garikipati, Recent advances in the analysis and numerical simulation of strain localization in inelastic solids, in: D.R.J. Owen, E. Oñate, E. Hinton (Eds.), Proceedings of Computational Plasticity IV, CIMNE, Barcelona, Spain, 1995, pp. 547–561.
[44] R.I. Borja, A finite element model for strain localization analysis of strongly discontinuous fields based on standard Galerkin approximation, Comput. Methods Appl. Mech. Engrg. 190 (2000) 1529–1549.
[45] R.I. Borja, R.A. Regueiro, Strain localization of frictional materials exhibiting displacement jumps, Comput. Methods Appl. Mech. Engrg. 190 (2001) 2555–2580.
[46] R.A. Regueiro, R.I. Borja, Plane strain finite element analysis of pressure sensitive plasticity with strong discontinuity, Int. J. Solids Struct. 38 (2001) 3647–3672.
[47] J.C. Simo, Numerical analysis and simulation of plasticity, in: P.G. Ciarlet, J.L. Lions (Eds.), Handbook of Numerical Analysis, vol. VI, North Holland, The Netherlands, 1998, pp. 183–499.
[48] E.H. Lee, Elastic-plastic deformation at finite strains, J. Appl. Mech. (1969) 1–6.
[49] Y.F. Dafalias, Plastic spin: necessity or redundancy?, Int. J. Plast. 14 (1998) 909–931.
[50] G.N. Wells, L.J. Sluys, Analysis of slip planes in three-dimensional solids, Comput. Methods Appl. Mech. Engrg. 190 (2001) 3591–3606.
[51] R.I. Borja, R.A. Regueiro, T.Y. Lai, FE modeling of strain localization in soft rock, J. Geotech. Geoenviron. Engrg., ASCE 126 (2000) 335–343.
[52] C. Miehe, Aspects of the formulation and finite element implementation of large strain isotropic elasticity, Int. J. Num. Meth. Engrg. 37 (1994) 1981–2004.
[53] C. Miehe, Comparison of two algorithms for the computation of fourth-order isotropic tensor functions, Comput. Struct. 66 (1998) 37–43.
[54] R.I. Borja, Plasticity Modeling and Computation, Lecture Notes, Stanford University, California, USA, 2002.
[55] R.I. Borja, K.M. Sama, P.F. Sanz, On the numerical integration of three-invariant elastoplastic constitutive model, Comput. Methods Appl. Mech. Engrg., in press.
[56] D.C. Drucker, W. Prager, Soil mechanics and plastic analysis or limit design, Quart. Appl. Math. 10 (1952) 157–165.
[57] P.V. Lade, J.M. Duncan, Elastoplastic stress–strain theory for cohesionless soil, J. Geotech. Engrg. Div., ASCE 101 (1975) 1037–1053.
[58] H. Matsuoka, T. Nakai, Stress-deformation and strength characteristics of soil under three different principal stresses, Proc. JSCE 232 (1974) 59–70.